PARTICLE PHYSICS AND COSMOLOGY

John Ellis

Theoretical Physics Division, CERN
CH-1211 Geneva 23

Lectures at the Brazilian School of Cosmology and Gravitation
July 1995

1. The Early Universe and the Standard Model

1.1. The first second - a general overview

To understand the very early history of our Universe, we need to understand elementary particles and their interactions. This is because, according to standard Big Bang Cosmology, during the first second the typical thermal energies of the constituents of the Universe were above 1 MeV, i.e., above the rest mass of the electron and at temperatures where nuclei dissolve into protons and neutrons. Back at around 10^{-6} to 10^{-5} s after the start of the Big Bang , protons and neutrons would themselves have been dissolved into their constituent quarks. The previous event of note was around 10^{-10} s, when the weak and electromagnetic interactions would have had comparable strengths, and hence been effectively unified as in the Standard Model of particle physics. The physics involved so far is well established and tested at accelerators: going back earlier in time requires more progressively more speculation. Sometime between 10^{-10} and 10^{-12} s, the particles of the Standard Model would have lost their masses as the electroweak vacuum was heated up and its symmetry restored. The matter of the Universe may have been created at any time between this electroweak phase transition and the phase transition around 10^{-35} s or so when the expected grand unified symmetry would have been restored. This may also be when cosmological inflation took place, according to which the present density of the Universe is essentially critical. This requires most of the suff in the Universe to be non-baryonic Dark Matter, for which the most plausible candidates may be neutrinos, present in the Standard Model but endowed with masses by grand unification, and/or the lightest supersymmetric particles.

To understand the framework for this sequence of events, it is useful to review first some basic facts about mass, energy, temperature and time in the early Universe. Like any gas, the constituents of the Universe have generally cooled as it expanded, with temperature $T \propto a^{-1}$, where a is the scale factor, during the adiabatic expansion that has dominated most of the Universe's history. While the cosmic gas is composed of relativistic particles, which is the case for most of the first second, the age

$$t \propto a^2 \propto T^{-2} \tag{1.1}$$

Numerically, the temperature of the Universe would have been about 10^{10} K when its age was 1s. This corresponds to thermal energies of about 1 MeV, comparable to the electron mass 0.511 MeV, whereas the proton mass of 938 MeV (about 1 GeV) corresponds to $T \sim 10^{13}$ K. The basic time/temperature relation (1.1) can be written as

$$t(s) = 0(1)/T(MeV)^2 \tag{1.2}$$

with the constant of proportionality depending on the number of particle species.

The mathematical framework for this physical picture is provided by the basic equations of Friedman-Robertson-Walker cosmology [1], in particular the equation

$$\left(\frac{\dot{a}}{a}\right)^2 + \frac{k}{a^2} = \frac{8\pi\, G_N}{3}\,\rho \tag{1.3}$$

which determines the Hubble expansion rate $H \equiv \dot{a}/a$. The second term on the left-hand side is the curvature term: the present Hubble expansion rate is close to that for a flat $k = 0$ Universe, for which the explanation may be inflation. On the right-hand side, we find Newton's constant $G_N \equiv 1/m_P^2$ where $m_P \simeq 1.22 \times 10^{19}$ GeV is the Planck mass, and ρ denotes the energy density. If $k = 0$, the Universe has the critical density $\rho = \rho_c$ and

$$H = \sqrt{\frac{8\pi\ G_N}{3}\ \rho_c} \tag{1.4}$$

where $\rho_c \simeq 2 \times 10^{-29} h^2 g cm^3$, with $h = H/(100 km s^{-1} Mpc^{-1})$.

For relativistic particles in thermal equilibrium [2],

$$\rho \simeq \frac{\pi^2}{30}\ T^4 g\ :\ g = \#_B + \frac{7}{8}\#_F \tag{1.5}$$

where in the Standard Model the number of boson particle states (see Lectures 2 and 3)

$$\#\mathrm{B} \ = \ \underset{(\mathrm{Higgs})}{4} \ + \ \underset{(\mathrm{Gluons})}{(8\times 2)} \ + \ \underset{(\mathrm{electroweak\ gauge})}{(4\times 2)} \ = \ 28 \tag{1.6}$$

and the number of fermion particle states

$$\#_F = 30\ N_G \tag{1.7}$$

where N_G is the number of matter generations. We also recall that for relativistic particles the pressure

$$p = \frac{1}{3}\rho \tag{1.8}$$

and that the number densities of bosons and fermions are

$$n_{B,F}(\underline{k}, T) = \frac{\#_{B,F}}{(2\pi)^3}\ \frac{1}{\exp(|\underline{k}|/T) \mp 1} \tag{1.9}$$

We have been assuming that thermal equilibrium was established in the early Universe: is this plausible? To answer this question, we should compare the Hubble expansion rate $H \sim T^2/m_P$ with typical interaction rates

$$\Gamma \ \sim \ \underset{(1 \leftrightarrow 2\ \mathrm{particles})}{\alpha T} \ , \ \underset{(2 \leftrightarrow 2\ \mathrm{particles})}{\alpha^2 T} \tag{1.10}$$

where (for example) the latter is obtained by estimating a typical thermal cross-section $\sigma(T) \sim \alpha^2/T^2$, where α is the fine structure constant, and using the fact that any relativistic particle number density $n(T) \sim T^3$. Equilibrium is maintained if $H \lesssim \Gamma$, i.e.,

$$T \lesssim \alpha m_P \tag{1.11}$$

However, interactions do drop out of equilibrium if they are mediated by massive particles. For example, for weak interactions mediated by massive W bosons in the Standard Model , $\sigma_W(T) \sim \alpha^2 T^2/m_W^4$ when $T \ll m_W$. Hence

$$\Gamma_W(T) \equiv \sigma_W(T) n(T) \sim \frac{\alpha^2 T^5}{m_W^4} < H \sim \frac{T^2}{m_P} \tag{1.12}$$

when

$$T \sim (m_W^4/m_P \alpha^2)^{1/3} \sim 1 \text{ MeV} \tag{1.13}$$

Therefore the weak interactions are believed to have maintained equilibrium during all the first second, except perhaps at the very beginning of the Big Bang [3].

It is useful to recall the effective horizon size $a_H = 2c.t$ of the Universe at different epochs during its expansion. At the quark-hadron transition when $T_c^{QCD} \simeq 150$ MeV, $t_c^{QCD} \simeq 2 \times 10^{-6}$ s and $a_H \simeq 9$ km, which has now expanded to about 1/2 ly. At the electroweak transition when $T_c^{EW} \simeq 150$ GeV, $t_c^{EW} \simeq 2 \times 10^{-12}$ s and $a_H \simeq 6.3$ mm, which expanded to 6m at t_c^{QCD}, and has expanded to about 20 astronomical units now.

1.2. Electroweak unification

In the laboratory, we see as force cariers the massless photon γ and the massive $W^{\pm}(\sim 80$ GeV) and Z^0 (91.1884(22) GeV). Correspondingly, electromagnetic forces have infinite range, whilst the weak forces have a short range $\sim 10^{-16}$ cm $\sim m_{W,Z}^{-1}$. Why are the γ and W/Z masses so different, given the similarities in their spins (1) and couplings ($\alpha_W \sim 1/30$ cf. $\alpha_{em} \sim 1/137$)? The elementary particles - quarks and leptons - on which the electroweak forces act are displayed below together with their masses:

Quarks	$\begin{pmatrix} u \\ d \end{pmatrix}$	$\begin{matrix} \sim 5 \text{ MeV} \\ \sim 8 \text{ Mev} \end{matrix}$	$\begin{pmatrix} c \\ s \end{pmatrix}$	$\begin{matrix} \sim 1.5 \text{ GeV} \\ \sim 0.15 \text{ GeV} \end{matrix}$	$\begin{pmatrix} t \\ b \end{pmatrix}$	$\begin{matrix} \sim 170 \text{ GeV} \\ \sim 5 \text{ GeV} \end{matrix}$
Leptons	$\begin{pmatrix} \nu_e \\ e \end{pmatrix}$	$\begin{matrix} \lesssim 4.5 \text{ eV} \\ \sim \frac{1}{2} \text{ MeV} \end{matrix}$	$\begin{pmatrix} \nu_\mu \\ \mu \end{pmatrix}$	$\begin{matrix} \lesssim 0.16 \text{ MeV} \\ \sim 0.1 \text{ GeV} \end{matrix}$	$\begin{pmatrix} \nu_\tau \\ \tau \end{pmatrix}$	$\begin{matrix} \lesssim 23 \text{ MeV} \\ \sim 1.78 \text{ GeV} \end{matrix}$

(1.14)

where the matter particles are paired in doublets of electroweak isospin. The upper limits on the neutrino masses are discussed in Lecture III, together with grand unified ideas about their possible magnitudes that suggest the ν_τ is a good candidate for the Hot Dark Matter discussed in Lecture 5. LEP experiments tell us that there are no more than three light neutrino species, as assumed in conventional Big Bang nucleosynthesis calculations (see Lecture II) and hence presumably three charged leptons. LEP data test and verify the electroweak sector of the Standard Model with a precision of a few per mille, as discussed in Section I.3.

To accommodate the above-mentioned gauge bosons using SU(2)× U(1) gauge symmetry [4], we need two gauge boson kinetic terms

$$\mathcal{L}_G = -\frac{1}{4} (G_{\mu\nu} G^{\mu\nu}) - \frac{1}{4} (F_{\mu\nu} F^{\mu\nu}) \tag{1.15}$$

where

$$F_{\mu\nu} \equiv \partial_\mu B_\nu - \partial_\nu B_\mu \tag{1.16}$$

for the U(1) of the electroweak hypercharge, and where

$$G_{\mu\nu a} \equiv \partial_\mu W_{\nu a} - \partial_\nu W_{\mu a} + ig\epsilon_{abc} W_{\mu b} W_{\nu c} \tag{1.17}$$

for the SU(2) of electroweak isospin. Expanding the latter, we obtain three-boson and four-boson interactions, as well as the bilinear terms.

The fermion kinetic terms in the Standard Model take the form

$$\mathcal{L}_F = -\sum_{f,L,R} i\left[\bar{f}_L \gamma^\mu D_\mu f_L + \bar{f}_R \gamma^\mu D_\mu f_R\right] \tag{1.18}$$

where the covariant derivative

$$D_\mu = \partial_\mu - ig\frac{\tau_a}{2} W_{\mu a} - ig' Y B_\mu \tag{1.19}$$

Note that the gauge interactions conserve helicity, that the term proportional to τ_a is absent for the f_R, reflecting the violation of parity, and that the values of the hypercharges Y will be fixed later. The g and g' are the gauge couplings for the SU(2) and U(1) gauge group factors, respectively. Expanding the fermion kinetic terms, we find in addition to bilinear terms also trilinear terms, in which a fermion emits a gauge boson while conserving its helicity.

We also need a scalar field, called the Higgs field ϕ, which is a doublet of electroweak SU(2), and has the kinetic term

$$\mathcal{L}_\phi = -|D_\mu \phi|^2 \tag{1.20}$$

Expanding this, we obtain, in addition to the usual bilinear terms, also trilinear terms with one gauge boson coupled to two fields ϕ, and quadrilinear terms with two boson fields coupled to two fields ϕ. The scalar field ϕ is also coupled to the fundamental quarks and leptons via what are called Yukawa terms

$$\mathcal{L}_Y = -\sum_{f,f'} \left[h_{ff'} \bar{f}_L \phi f'_R + h^*_{ff'} \bar{f}_R \phi^\dagger f_L\right] \tag{1.21}$$

Here $h_{ff'}$ is an arbitrary matrix in flavour space. Note that these ϕ interactions flip helicity from left to right. When the Higgs field ϕ acquires a vacuum expectation value (v.e.v.), which it will do shortly, these Yukawa terms may be expanded to give masses $m_f \propto h_{ff'}$, as well as Higgs-fermion-antifermion couplings.

The final part of the Standard Model Lagrangian is the Higgs potential

$$\mathcal{L}_V \equiv -V(\phi) \; : \quad V(\phi) = -\mu^2 \phi^\dagger \phi + \frac{\lambda}{2}(\phi^\dagger \phi)^2 \tag{1.22}$$

This can be expanded to give a mass term and quadrilinear interactions. You can regard the field ϕ as resembling a glorified harmonic oscillator, with the second term in the potential corresponding to an anharmonic term. The energy of the theory is minimized by going to the lowest point in the effective potential, which determines the vacuum of the theory. Since the quadratic (harmonic) term has a negative coefficient, the origin $\phi = 0$ is unstable, and the minimum of the potential is located at

$$\langle 0|\phi|0\rangle = \langle 0|\phi^\dagger|0\rangle = v\begin{pmatrix} 0 \\ 1/\sqrt{2} \end{pmatrix} \; : \; v^2 = \frac{\mu^2}{2\lambda} \tag{1.23}$$

The Higgs potential is sketched in Fig. 1, where we see that there is a non-trivial set of minima which are all at the same height. All of these vacua are equivalent, and it is a choice of one of them which breaks the symmetry. The appearance of this v.e.v. means that the electroweak $SU(2) \times U(1)$ symmetry is spontaneously broken, since the Higgs field is not invariant under the electroweak symmetry transformations. It should be noted here that it is convention which puts the v.e.v. v of the Higgs field in the lower part of the doublet.

It is this symmetry breaking which provides the mechanism for mass generation in the Standard Model . If we substitute

$$\phi = \langle 0|\phi|0\rangle + \hat{\phi} \tag{1.24}$$

into the Higgs kinetic term $\mathcal{L}_\phi$, we find that the quadrilinear $\phi^2 v^2$ terms now give us quadratic terms

$$\mathcal{L}_\phi \ni -\frac{g^2 v^2}{2} W_\mu^+ W^\mu - g'^2 \frac{v^2}{2} B_\mu B^\mu + g g' v^2 B_\mu W_\mu^3 - g^2 \frac{v^2}{2} W_\mu^3 W_\mu^3 \tag{1.25}$$

The first of these gives a mass to the charged $W^\pm$ bosons

$$m_W = g \frac{v}{2} \tag{1.26}$$

The other three terms give masses to the neutral gauge bosons B_μ and W_μ^3. Recall that a gauge boson mass term $A_\mu A^\mu$ is not in gauge invariant by itself: however, since we have obtained these terms from what was originally a gauge-invariant kinetic term for the Higgs fields, this mechanism of mass generation is in fact gauge-invariant.

The neutral gauge boson masses require a bit more discussion than those of the charged bosons. We see in Eq. (1.25) above a matrix of terms coupling the fields B_μ and W_μ^3

$$\begin{pmatrix} \frac{g'^2 v^2}{2} & -\frac{g g' v^2}{2} \\ -\frac{g g' v^2}{2} & \frac{g^2 v^2}{2} \end{pmatrix} \tag{1.27}$$

It is easy to check that, when diagonalised, this matrix gives one massive combination

$$Z_\mu^0 \equiv \frac{g W_\mu^3 - g' B_\mu}{\sqrt{g^2 + g'^2}} \; : \; m_Z = \frac{1}{2}\sqrt{g^2 + g'^2}\; v \tag{1.28}$$

which we will soon interpret as the Z^0 boson explored at LEP and elsewhere, and one massless combination,

$$A_\mu \equiv \frac{gW_\mu^3 + g'B_\mu}{\sqrt{g^2 + g'^2}} \tag{1.29}$$

which is the familiar photon of electrodynamics. We see that the photon is a combination of W_μ^3 and B_μ, and therefore couples to the combination

$$Q_{em} = I_3 + Y \tag{1.30}$$

of weak isospin and hypercharge. This tells us how to choose the values of the hypercharges for the different fields: they must be chosen such that, when combined with the values of I_3, they together give the known electromagnetic charges of the elementary particles. The photon has a coupling of strength

$$e = \frac{gg'}{\sqrt{g^2 + g'^2}} \tag{1.31}$$

which is a combination of the SU(2) coupling g and the U(1) coupling g'. It is convenient to parametrize these couplings in terms of a mixing angle θ_W, which is related to the couplings g' and g by

$$\tan\theta_W = \frac{g'}{g}\ , \quad \cos\theta_W = \frac{g}{\sqrt{g^2 + g'^2}}\ , \quad \sin\theta_W = \frac{g'}{\sqrt{g^2 + g'^2}} \tag{1.32}$$

Referring back to the previous expressions for $m_{W^\pm}$ and m_{Z^0}, we find the following relationship between their masses

$$\sin^2\theta_W = 1 - \frac{m_W^2}{m_Z^2} \tag{1.33}$$

We shall shall call θ_W the electroweak mixing angle.

It is a useful exercise to check that the familiar low-energy four-fermion weak interactions can be obtained by the exchanges of massive $W^\pm$ and Z^0 bosons. In the case of the $W^\pm$ exchanges, we recover

$$\frac{1}{4}\,\mathcal{L}_{eff}^{CC} \equiv \frac{G_F}{\sqrt{2}}\left(J_\mu^+ J^{\mu -}\right) \tag{1.34}$$

where

$$J_\mu^+ = \bar{\nu}_L \gamma_\mu \ell_L + \ldots \tag{1.35}$$

with the normalisation

$$\frac{G_F}{\sqrt{2}} = \frac{g^2}{8m_W^2} \;:\; m_W = \frac{gv}{2} \tag{1.36}$$

This expression fixes the overall normalisation of the v.e.v. of the Higgs field

$$v = \left(\sqrt{2}G_F\right)^{-1/2} \tag{1.37}$$

Similarly, the exchange of the massive Z^0 boson gives us an interaction of the form

$$\frac{1}{4}\,\mathcal{L}_{eff}^{NC} = \frac{G_F}{\sqrt{2}}\left(\rho\; Z J_\mu^{NC} J^{NC\mu}\right) \;:\; \rho = 1 \tag{1.38}$$

where the neutral current is given by

$$J_\mu^{NC} = J_\mu^3 - \sin^2\theta_W\; J_\mu^{em} \tag{1.39}$$

as can be seen from Eq. (1.28) above. The different overall coupling strength

$$\sqrt{g^2 + g'^2} \tag{1.40}$$

and mass of Z^0 boson, Eq. (1.28), combine to give the same strength to the neutral current interactions as for the charged-current interactions, namely $\rho = 1$ in the language of Section 1.2. This is a characteristic prediction of our assumption that the Higgs field ϕ has electroweak isospin $I = 1/2$. Other choices of isospin would have given us a different ratio for the $W^\pm$ and Z^0 boson masses, and hence for the relative strength of the charged-current and neutral-current interactions [5].

1.3. Testing electroweak unification

So far, our discussion of the Z^0 peak has been at the classical or "tree" level, which can be regarded as the first step in the systematic approximation scheme called perturbation theory. The expansion parameter in this perturbation theory is the electroweak analogue of the fine structure constant

$$\alpha_2 \equiv \frac{g^2}{4\pi} \simeq \frac{1}{30} \tag{1.41}$$

Up to now, we have just been calculating the tree-level amplitudes shown in Fig. 2, which are

$$A \sim \alpha_2 \tag{1.42}$$

and thus make contributions to the cross-sections that are of order α_2^2. The next step in the approximation scheme is to calculate one-loop quantum corrections like those shown in Fig. 3. The diagram in Fig. 3a is known as a vacuum polarization diagram, that in Fig. 3b is a typical vertex correction, that in Fig. 3c is called a box diagram. Adding these to the previous tree-level amplitudes A, we find

$$\sigma = |A + \delta A|^2 \simeq |A|^2 + 2\mathrm{Re}(A\,\delta A^*) \tag{1.43}$$

providing a correction to the cross-section that is of order α_2^3.

Do not worry, you are not expected to be able to calculate these diagrams. If you did, you would find that generic one-loop diagrams are infinite. In a renormalisable (i.e., calculable) theory such as the Standard Model [6], all these infinities can be absorbed into the physical values of a finite number of measurable input parameters. In the case of the electroweak sector of the Standard Model , these are α_{em} (the fine structure constant), m_{Z^0} (measured very precisely at LEP), and G_μ (the Fermi μ decay constant). It is also often convenient to keep as an auxiliary parameter $\sin^2\theta_W \equiv 1 - m_W^2/m_Z^2$, which is closely related to the ratio of SU(2) and U(1) couplings, as discussed in Section I.2.

It was pointed out many years ago by Veltman [7] and others [8] that the one-loop diagrams were sensitive to the masses of unseen particles, such as the top quark and the Higgs boson. For example, the masses of the $W^\pm$ and Z^0 bosons are given by

$$m_W^2 \sin^2\theta_W = m_Z^2 \cos^2\theta_W \sin^2\theta_W = \frac{\pi\alpha}{\sqrt{2}G_\mu}\,(1 + \Delta r) \tag{1.44}$$

where Δr is a quantum correction whose structure we now discuss. As has already been mentioned, the top quark is essential in the Standard Model . Indeed, the gauge symmetry structure of the electroweak theory would be lost, and renormalisability, i.e., calculability, with it, if the top quark were not present to complete the isospin doublet inhabited by the bottom quark. The difference between m_t and m_b is a measure of electroweak isospin symmetry breaking, which shows up at the one-loop level in vacuum polarisation diagrams. They make a contribution to the above-mentioned quantum correction Δr of the form

$$\Delta r \ni \frac{3G_\mu}{8\pi^2\sqrt{2}}\; m_t^2 \tag{1.45}$$

in the limit $m_t \gg m_b$. This quadratic dependence on m_t gives one an experimental handle on the mass of the unseen top quark.

Similarly, since the Higgs boson is essential to spontaneous symmetry breaking, and the theory would not be renormalisable, i.e., calculable, without it, the one-loop diagrams are also sensitive to its presence, and hence its mass

$$\Delta r \ni \frac{\sqrt{2}G_\mu}{16\pi^2}\, m_W^2 \left\{ \frac{11}{3} \ln m_H^2/m_W^2 - \ldots \right\} \text{ for } m_H \gg m_W \tag{1.46}$$

M_Z	91.1884	$\pm$	0.0022	GeV
Γ_Z	2.4963	$\pm$	0.0032	GeV
σ_h^0	41.488	$\pm$	0.078	nb
R_L	20.788	$\pm$	0.032	
A_{FB}^l	0.0172	$\pm$	0.0012	
A_τ	0.1418	$\pm$	0.0075	
A_l	0.1390	$\pm$	0.0089	
R_b	0.2219	$\pm$	0.0017	
R_c	0.1543	$\pm$	0.0074	
A_{FB}^b	0.0999	$\pm$	0.0031	
A_{FB}^c	0.0725	$\pm$	0.0058	
$\sin^2\theta_{eff}(Q_{FB})$	0.2325	$\pm$	0.0013	
M_W	80.26	$\pm$	0.16	GeV
$\sin^2\theta_{eff}(A_{LR})$	0.23049	$\pm$	0.00050	

Table 1

Note, however, that the sensitivity to the Higgs mass is only logarithmic, which makes it more difficult to extract some information on it from the available electroweak data. Moreover, as seen in Fig. 4, the top and Higgs contributions to Δr can compensate each other. If, say, the quantum correction Δr were measured to have a value of 0.05, one could say that m_t was in the range 100-150 GeV, for m_H between 10 and 1000 GeV. However, one could not be more precise without additional information, either in the form of a determination of m_t or by having available other precision measurements sensitive to different combinations of m_t and m_H. As shown in Table 1, LEP does indeed provide us with a large number of precision electroweak measurements [9], including measurements of the total Z^0 decay width, cross-section measurements on the Z^0 peak, various forward-backward asymmetries, and determinations of individual partial Z^0 decay widths, which are sensitive to m_t and m_H in different ways.

The current state of play in the sensitivity of precision electroweak measurements to m_t and m_H can be summarised as follows [10]. If M_H is left as a free parameter, then the prefered range of m_t is

$$m_t = 155 \pm 14 \text{ GeV} , \tag{1.47}$$

to be compared with the CDF and D0 measurements:

$$m_t = 181 \pm 12 \text{ GeV} . \tag{1.48}$$

Combining these, one finds

$$m_t = 172 \pm 10 \text{ GeV} . \tag{1.49}$$

The preferred range of m_t is correlated positively with the value of m_H. However, the data tend to prefer a small value of m_H, close to the present direct lower limit of about 65 GeV:

$$M_H = 76^{+152}_{-50} \text{ GeV} . \tag{1.50}$$

Based on these indications from the precision electroweak data including quantum corrections, I personally would give 3-1 odds that $m_H < 300$ GeV.

2. The Standard Model at Finite Temperature

2.1. The strong interaction sector of the Standard Model

According to the naïve quark model, strongly-interacting baryonic particles such as the nucleons (proton and neutron) are made out of three quark constituents each. For example, the proton contains two constituent u quarks and one constituent d quark, whilst the neutron contains two constituent d quarks and one constituent u quark. It is easy to see that according to this model, the quarks must have fractional charges

$$\left.\begin{array}{l} 1 = Q_p = 2Q_u + Q_d \\ Q_u - Q_d = 1 \end{array}\right\} \Rightarrow \begin{array}{l} Q_u = \frac{2}{3} \\ Q_d = -\frac{1}{3} \end{array} \tag{2.1}$$

This naïve quark model leads to certain puzzles, which are displayed most clearly by the Δ baryon, which is an excited state of the nucleons. One of the Δ baryons is doubly-charged and, according to the naïve quark model, is made out of three constituent u quarks, all with their spins pointing in the same direction. However, we are accustomed from atomic and nuclear physics to expect that the lowest-lying states lie in a relative S-wave. In the case of the Δ^{++}, this would lead to an apparent paradox, since the three u quarks which have to be in identical states, which is forbidden by the Pauli principle. The resolution of this puzzle which is taken up by the Standard Model is that each flavour of quark comes in three identical varieties, whimsically called colours [11].

As we shall see later, the naïve quark model may not be the best guide to the composition of strongly-interacting particles. However, experiments give us many other reasons for believing in the colour degree of freedom. For example, at high centre-of-mass energies above about 2 GeV, the total cross-section for $e^+e^- \to$ hadrons is much larger than in the naïvequark model without colour

$$\frac{\sigma(e^+e^- \to \text{hadrons})}{\sigma(e^+e^- \to \mu^+\mu^-)} \simeq \sum_{u,d,s} Q_q^2 = \frac{2}{3} \tag{2.2}$$

Experiments indicate that between about 2 GeV and about 4 GeV, this ratio is close to 2, the ratio expected if each u, d and s quark flavour comes in three distinct colours. The same pattern persists above 4 GeV, where the total $e^+e^- \to$ hadrons cross-section is about three times larger than that expected in the naïve quark model with charm c but without colour. A similar feature is seen in $\tau \to \nu_\tau +$ hadrons decays, which are about three times more frequent than $\tau \to \nu_\tau + e + \bar{\nu}_e$ decays, as would be expected if the τ decays into $\bar{u}d$ pairs with three different colours. An additional reason for believing in colour comes from the measured rate of $\pi^0 \to \gamma\gamma$ decay, which has an amplitude proportional to that number of colours. The experimental data indicate

$$N_c = 2.987 \pm 0.016 \tag{2.3}$$

We therefore assume $N_c = 3$.

In the Standard Model , the strong interactions are described by a gauge theory analogous to that used for the electroweak interactions. It acts on the three colour degrees of freedom via a non-Abelian group called SU(3) in a theory known as Quantum Chromodynamics, or QCD. According to this theory, the quark kinetic terms are given by

$$\mathcal{L}_q = -\sum_q i(\bar{q}_L \gamma^\mu D_\mu q_L + \bar{q}_R \gamma^\mu D_\mu q_R) \tag{2.4}$$

where

$$D_\mu = \partial_\mu - i g_3 \frac{\lambda_a}{2} G^a_\mu \tag{2.5}$$

is a gauge-covariant derivative, with g_3 the strong coupling, λ_a an SU(3) representation matrix, and the G^a_μ representing eight boson fields called gluons. Expanding these quark kinetic terms, we find, in addition to bilinear terms describing quark propagation, also vertices in which quarks emit or absorb a gluon while conserving helicity. Note that the q_L and q_R are placed in identical 3 representations of the strong colour SU(3) group. This means that they conserve parity P, charge conjugation C, and their combination known as CP.

In addition to the quark kinetic terms, QCD also contains gluon kinetic terms which take the form

$$\mathcal{L}_G = -\frac{1}{4} (G_{\mu\nu a} G^{\mu\nu a}) \tag{2.6}$$

where

$$G_{\mu\nu a} = \partial_\mu G_{\nu a} - \partial_\nu G_{\mu a} + i g_3 f_{abc} G_{\mu b} G_{\nu c} \tag{2.7}$$

Here g_3 is again the strong coupling, and the f_{abc} are the non-Abelian structure constants of the group SU(3). Expanding these gluon kinetic terms, we encounter bilinear terms and also trilinear and quadrilinear gluon self-interactions, analogous to those of the electroweak gauge bosons. The gluon kinetic terms written above also conserve P, C, and CP. However, there is an additional possible term in the QCD Lagrangian [12] which could violate P and CP.

One of the most remarkable features of QCD is its property of **asymptotic freedom**. As we have already seen, quantum effects are very important in field theory. Specifically, in the case of QCD they cause the strong coupling g_3 to decrease as a function of the energy scale at which it is measured. At the leading one-loop order, the variation of the strong equivalent of the fine structure constrant is described approximately by [13]

$$\alpha_3(Q) \equiv \frac{g_3^2(Q)}{4\pi} = \frac{12\pi}{(33 - 2N_q) \ln Q^2/\Lambda^2} + \ldots \tag{2.8}$$

Here, N_q is the number of quark flavours with masses $m_q \ll Q$, the energy scale, and Λ is an intrinsic mass-energy scale of the strong interactions. The dots in Eq. (2.8) represent higher-order

terms which have also been calculated, and do not alter the fact that the strong coupling becomes weaker at higher energies $Q \ll \Lambda$. By the uncertainty principle, such high energies correspond to short distances, and Eq. (2.8) tells us that quarks behave almost as free particles at sufficiently short distances. Figure 5 shows a compilation of data on $\alpha_3(Q)$ as a function of the energy scale Q, showing clear evidence that it decreases as the effective energy scale Q increases. These data indicate the following value for the intrinsic mass-energy scale of the strong interactions

$$\Lambda \simeq 200 \text{ MeV} \times 2^{0\pm1} \tag{2.9}$$

Interpreted naïvely, Eq. (2.8) suggests that the strong coupling becomes really strong at energies $Q \lesssim 1$ GeV, with an apparent divergence at $Q = \Lambda$. The leading-order formula (2.8) cannot be trusted when the strong coupling becomes really strong, but this feature is highly suggestive of confinement.

Quarks and gluons have never been seen isolated. They are only known to exist confined within strongly interacting particles (hadrons) such as baryons and mesons. According to the naïve quark model, mesons such as the π can be regarded as $q\bar{q}$ bound states. The π^+, π^0, and π^- are the lightest hadronic particles, with masses below 140 MeV. Their lightness is related by chiral symmetry to that of the u and d quarks. According to the theory of QCD [14],

$$m_\pi^2 \simeq \frac{\langle 0|\bar{q}q|0\rangle}{f_\pi^2}\ (m_u + m_d) \tag{2.10}$$

where $\langle 0|\bar{q}q|0\rangle$ is the value of the $q\bar{q}$ condensate in vacuo, and f_π is the pion decay constant which parametrises the coupling of the charged pions to the $W^\pm$. Equation (2.10) tells us that

$$m_\pi^2 \sim \Lambda_{QCD} \times m_q \tag{2.11}$$

Putting in all the appropriate numerical factors, this relation is used to estimate [14]

$$m_u \sim 5 \text{ MeV}\ , \quad m_d \sim 8 \text{ MeV} \tag{2.12}$$

These quark masses are much smaller than those previously favoured in the naïve quark model, and are not so much larger than m_e. An analogous calculation based on the $K^+ = (u\bar{s})$ and $K^0 = (d\bar{s})$ masses yields the estimate $m_s \simeq 150$ MeV. As has already been mentioned, according to the naïve quark model, the baryons are interpreted as qqq bound states, and the observed masses $m_{p,n} \simeq 940$ MeV are intepreted as indicating that the constituent quark masses are of order 300 MeV. However, according to chiral symmetry in QCD [15], the baryon masses are not directly related to the light quark masses, Eq. (2.12), but instead

$$\begin{aligned} m_{p,n} &\sim \langle 0|\bar{q}q|0\rangle^{1/3} \sim \langle 0|G^a_{\mu\nu}G^{\mu\nu}_a|0\rangle^{1/4} \\ &\sim \Lambda_{QCD} \end{aligned} \tag{2.13}$$

where $\langle 0|G^a_{\mu\nu}G^{a\mu\nu}|0\rangle$ is the gluon-gluon condensate in vacuo.

As already mentioned, both the $q\bar{q}$ condensate $\langle 0|\bar{q}q|0\rangle$ and the gluon-gluon condensate $\langle 0|G^a_{\mu\nu}G^{a\mu\nu}|0\rangle$ are non-zero at low temperatures and pressures. However, they are believed to

decrease and go to zero at one or more phase transition temperatures of order 150 MeV, as mentioned in Lecture 1. Just below this temperature, hadrons are described as a gas whose energy density is dominated by the π^+, π^0, π^- with relatively few p, n, since the latter have abundances suppressed by Boltzmann factors.

Figure 6 sketches the qualitative form of the boundary between this low-temperature hadron phase of QCD, and the quark/gluon phase which appears at high temperatures T and/or high values of the baryon chemical potential μ_B. The stable phase of strongly-interacting matter below and to the left of the indicated boundary is expected to consist of the familiar hadrons, whilst the stable phase above and to the right of the indicated boundary consists of deconfined quarks and gluons. It should be noted that superheating of the hadronic phase and/or supercooling of the quark/gluon phase would be possible if the transition between the two phases is first-order. This is expected to be the case for three light quark flavours, and may also be the case for the physical situation in which there are two very light quarks u and d and the strange quark s is estimated to have a mass around 150 MeV. Astrophysicists probe the quark-hadron phase boundary in two ways, as indicated in Fig. 6. There may be a quark-gluon phase in the core of certain neutron stars, at very high values of the baryon chemical potential μ_B and relatively low temperatures T. Of more direct interest at this School is the fact that the early Universe is believed to have cooled from a very high-temperature, low-μ_B phase down to low temperatures. In Lecture 2, we will discuss in more detail the possible order of the quark-hadron phase transition, and its possible implications for Big Bang nucleosynthesis.

2.2. General description of phase transitions

The most basic thermodynamic quantity [2] is the free energy F, which is defined in terms of the Hamiltonian H, the temperature $T \equiv 1/\beta$, and volume V by

$$e^{-F(T,V)/T} = Tr\, e^{-\beta H} \tag{2.14}$$

The free energy can be written in terms of the pressure p and the entropy S as follows:

$$F(T,V) = -Vp(T) = E(T,V) - T \cdot S(T,V) \tag{2.15}$$

At a phase transition, the free energy F (pressure p) is continuous, but changes occur in its derivatives and in one or more order parameters χ. We distinguish first-order and second-order phase transitions in which the change $\Delta\chi$ in the order parameter is either non-zero or zero, respectively. The generic natures of first- and second-order phase transitions are shown in Fig. 10. In the case of a first-order transition, Fig. 7a, the transition occurs as a jump in χ which results from quantum tunnelling through the indicated barrier. On the other hand, in a second-order phase transition, Fig. 7b, the order parameter χ varies continuously, and can be regarded as rolling classically down a hill from the unstable vacuum at $\chi = 0$ towards the stable vacuum at $\chi \neq 0$. The new vacuum with $\chi \neq 0$ forms via different processes in these two cases. In the case of a first-order transition, the dominant process is bubble nucleation, as indicated in Fig. 8a. A bubble region of the new vacuum is surrounded by the old vacuum with a wall in between. In the case of a second-order phase transition, the dominant mechanism is spinodal decomposition as illustrated in Fig. 8b. As the temperature T decreases, different parts of the medium may roll

to different non-zero values of the order parameter χ, which are separated by regions of values of χ where the potential is unstable. A key feature of first-order phase transitions is that the correlation length ξ remains finite, whereas it goes to infinity

$$\xi \to (T - T_c)^{-p} \; : \; p > 0 \tag{2.16}$$

in the case of second-order phase transition.

Since, as already mentioned, the quark-hadron phase transition may well have been first-order, we need to study the mechanism of bubble nucleation in more detail. The rate of bubble nucleation is given generically by an expression of the form

$$\Gamma \sim (\ldots) \exp\left(-\beta E_B\right) \tag{2.17}$$

where the exponent contains a factor of the classical bubble energy E_B, and we have indicated in parentheses a quantum prefactor that need not concern us here. Classical energetic considerations tell us that

$$E_B = \frac{-4\pi}{3} r^3 \cdot \Delta\rho + 4\pi r^2 \cdot \sigma \tag{2.18}$$

where the first is a volume term, r is the bubble radius, $\Delta\rho$ is the difference in energy density between the media inside and outside the bubble, and the second is a surface term with σ denoting the surface tension. The surface tension is just the contribution to the total free energy per unit of surface area which appears in the region of transition between the new and old vacua, represented by the wall in Fig. 8a. The classical bubble size r_B is obtained by extremising the energy in Eq. (2.18)

$$\frac{\partial E_B}{\partial r} = 0 \; : \; r_B = \frac{2\sigma}{\Delta\rho} \tag{2.19}$$

In this case, the classical bubble energy E_B is just given by

$$E_B = \frac{4}{3}\pi\sigma r_B^3 \tag{2.20}$$

Bubbles produced with $r < r_B$ will shrink and disappear after formation, whilst larger bubbles with $r > r_B$ will go and expand indefinitely. This yields the "Swiss cheese" picture of a phase transition shown in Fig. 9. The phase transition is completed when the expanding bubbles fill the whole of space.

2.3. Modelling the strong phase transition

As has already been mentioned, the pressure in the low-temperature hadron phase is determined essentially by the lightest degrees of hadronic freedom, namely the π^+, π^0, π^-

$$p_h = a_h T^4 \; : \; a_h = \frac{\pi^2}{90} \times 3 \tag{2.21}$$

In addition, the e, μ, ν and γ, which are inert under the strong interactions, also contribute to the total pressure felt by the Universe. On the other hand, the pressure in the high-temperature quark phase is given by

$$p_q = a_q T^4 \ : \ a_q = \frac{\pi^2}{90}\left[\frac{21}{2} \cdot N_q + 16\right] \tag{2.22}$$

where the first term comes from the $2(u, d)$ or $3(u, d, s)$ light quarks, and the second term is due to the eight gluons, each with two helicity states. In addition, there is the same contribution from the inert leptonic degrees of freedom. Comparing Eqs. (2.21) and (2.22), we see that there is apparently no temperature at which the pressures in the hadron and quark phases can be equal, which we recall from the previous section was a necessary condition at the critical temperature T_c of a phase transition. However, we have not yet incorporated all the strong interaction dynamics which confines quarks and gluons. One simple way of incorporating its essence has been proposed [16], namely to add to the pressure a so-called bag constant

$$\Delta p_q = -B \tag{2.23}$$

The bag constant can be regarded as an effective cosmological constant present outside hadrons. Equating the standard expression for the energy momentum tensor of a perfect fluid with that given by a bag constant,

$$\frac{p_h}{T^4} = a_h = a_q - \frac{B}{T^4} = \frac{p_q}{T^4} \tag{2.24}$$

where the fluid flow four-vector $u^\mu = (1, 0, 0, 0)$, we see that

$$T_c = \left(\frac{B}{(a_q - a_h)}\right)^{1/4} \tag{2.25}$$

in the presence of a bag constant. This is supposed to mimic the effect of the confinement potential. It is supposed to be present outside hadrons, but absent inside hadrons, so that quarks and antiquarks are bound inside mesons and qqq triplets are bound inside baryons. Adding this contribution to the pressure Eq. (2.22) in the quark phase, we see that it can become equal to that in the hadron phase given by Eq. (2.21)

$$T^{\mu\nu} = (\rho + p)u^\mu u^\nu - pg^{\mu\nu} = Bg^{\mu\nu} \tag{2.26}$$

where $u^\mu = (1, 0, 0, 0)$. The resulting vacuum energy density and pressure are

$$\rho_{vac} = -p_{vac} = B \tag{2.27}$$

in this simple model.

The pressure curves in the hadronic and quark phases are shown as solid lines in Fig. 10. They cross at the critical temperature T_c where the hadron and quark pressures are equal. Also shown

as dashed lines are possible superheating of the hadron phase up to a maximum superheating temperature T^+, and a supercooling curve for the quark phase down to a minimum supercooling temperature T^0. In the model of the previous paragraph, the quark/hadron phase transition is first-order, with the order parameter provided by the bag constant B. It follows from the discussion at the end of the previous section that a first-order phase transition is completed when the bubble nucleation rate becomes equal to the Hubble expansion rate. This condition can be written as

$$(H_c \simeq \frac{T_c^2}{m_P} = \frac{1}{t_c}) \simeq a_c^3 \; T_c^4 \exp(-\frac{E_B}{T}) \tag{2.28}$$

where the left-hand side is the Hubble expansion rate H_c at the critical temperature, the first term on the right-hand side is the volume of the Universe at the critical temperature T_c (critical time t_c), the second factor on the right-hand side is a dimensional factor representing the effects of quantum corrections, and the last factor in the exponential is the bubble energy discussed in Section II.5. In the case of the QCD phase transition, we can solve these equations to obtain

$$\frac{E_B}{T} \simeq \ln(t_c T_c)^4 \tag{2.29}$$

where

$$\frac{E_B}{T} \simeq \frac{64\pi}{3} \frac{\sigma^3}{L^2 T_c} \frac{1}{(t/t_c - 1)^3} \tag{2.30}$$

with σ again denoting the surface tension, and L the latent heat of the phase transition. The factors depending on time in the denominator on the right-hand side come from the fact that the difference between the pressures in the old and new phases must vanish when $t = t_c$, in which case the bubble radius and hence the bubble energy becomes infinite.

In order to estimate the temperature T_f and the time t_f when the QCD phase transition is completed, we need estimates of the surface tension σ and the latent heat L. Since QCD is a strongly-interacting theory in the neighbourhood of the critical temperature, it is difficult to calculate these quantities precisely. Some estimates have been made using phenomenological models and effective low-energy field theories [17]. However, the best estimates of σ and L are probably those from lattice gauge theory calculations, which suggest [18]

$$\frac{\sigma}{T_c^3} \simeq 0.1 \qquad \frac{L}{T_c^4} \simeq 10 \tag{2.31}$$

We see that the surface tension σ is rather small compared with the natural energy scale T_c. This combined with the relatively large latent heat L means that the amount of supercooling is expected to be very small [19]

$$1 - \frac{T_f}{T_c} \simeq 0.001 \tag{2.32}$$

Correspondingly, the bubble size is expected to be rather large [19]

$$r_f = \frac{2\sigma}{L(1 - T_f/T_c)} \sim \frac{\sigma}{L} \cdot \frac{L}{\sigma^{3/2}} \sim \frac{1}{\sigma^{1/2}} \simeq 20 \text{ to } 40 \text{ fm} \tag{2.33}$$

The basic reason why r_f is so large, much larger than an intrinsic strong interaction scale, is that the Hubble expansion rate $H \simeq T^2/m_P$ is so small. This is actually a necessary consistency condition for the reliability of the simple energetic analysis of bubble formation given in the previous section. We implicitly assumed there that the bubble wall was thin compared with the bubble radius. This thin-wall approximation is likely to be accurate for QCD, since the bubble-wall thickness is likely to be $\sim 1/\Lambda \sim 1fm$, which is much smaller than the critical bubble size $r_f \sim 30fm$. One can also calculate the typical distance between nucleation centres

$$\Delta r \sim 10^{-5} t_c \sim \text{few cm} \tag{2.34}$$

This gives the typical scale of inhomogeneities in the Universe after the quark/hadron phase transition. Although much larger than a natural strong-interaction scale, this scale of inhomogeneity is still much too small to have an appreciable effect on cosmological nucleosynthesis, as we discuss in the next two sections.

2.4. Inhomogeneous Big Bang nucleosynthesis

In recent years, this possibility has excited a lot of interest, mainly due to the possibility of a first-order QCD phase transition of sufficient strength to create inhomogeneities in the very early Universe that affect significantly primordial light element abundances [20]. The Universe could have been sufficiently lumpy at temperatures $T < 1.50$ MeV if the distance between nucleation sites of the new hadronic vacuum were large

$$\Delta r \gtrsim 0.5m \tag{2.35}$$

where the right-hand side represents the diffusion length of protons through the cosmological medium. In this case, neutrons would diffuse much further than protons, enabling the n/p ratio and η to vary in different parts of the Universe. As can be deduced from the discussion of the previous section, these possibilities would allow for different light element abundances. The question was then raised whether this flexibility would allow the Universe to be closed by baryons alone, thus obviating the need for non-baryonic dark matter.

The discussion of Section II.3 suggests that such a radical scenario is unlikely, given our knowledge of the quark/hadron phase transition. We recall that using the estimates [18]

$$\frac{\sigma}{T_c^3} \sim 0.1 \ , \quad \frac{L}{T_c^4} \sim 10 \tag{2.36}$$

of the QCD phase transition parameters given there, the typical separation between hadronic bubble nucleation sites was estimated as

$$\Delta r \sim \text{few cm} \tag{2.37}$$

which is much smaller than required above in Eq. (2.35). However, since the strong interactions are really strong in the neighbourhood of the critical temperature T_c, it is difficult to estimate the surface tension σ and the latent heat L very reliably. In particular, we cannot be absolutely sure that σ is not much larger than the estimate in Eq. (2.36), in which case the typical distance between nucleation sites could be in the interesting range given in Eq. (2.35). It should be reemphasized, though, that this possibility is disfavoured.

Independently of this particle physics argument, astrophysicists have also studied [21] whether such a radical inhomogeneous Big Bang nucleosynthesis scenario is compatible with astrophysical constraints on the light element abundances. The first difficulty with an $\Omega_B = 1$ Universe which emerged was the apparent overabundance of ^{7}Li. However, as discussed in the previous section, there is a question whether this might have been modified by a special depletion process in population II stars. We now know also that there is a problem with the abundance of ^{4}He in an inhomogeneous scenario. Regions with high baryon densities overproduce the heavier light elements, and this problem persists even if the ^{4}He bound is relaxed. Moreover, there is also a tendency to underproduce D in an inhomogeneous nucleosynthesis scenario, but this is a notoriously delicate element, as discussed in the previous section. However, if one takes all the astrophysical constraints at face value, then, as shown in Fig. 11, an $\Omega_B = 1$ Universe seems to be excluded [21]. There is very little room for deviation from the standard homogeneous Big Bang nucleosynthesis scenario, one still finds

$$\frac{n_B}{S} \simeq 3 \times 10^{-10} \tag{2.38}$$

and the scenario of a strongly first-order quark/hadron phase transition seems to be excluded by the weight of the astrophysical evidence as well.

2.5. Modelling the electroweak phase transition

There is a general effective description of the behaviour of an order parameter close to a critical temperature T_c, called the Landau mean-field expansion [22]. One introduces a parameter χ describing the order parameter, and writes down a general parametrization of the effective potential as a polynomial in χ

$$V_{eff}(\chi) = \frac{1}{2}\gamma(T^2 - T_0^2)\,\chi^2 - \frac{1}{3}\alpha T\chi^3 + \frac{1}{4}\lambda\chi^4 \tag{2.39}$$

In this expansion, α, γ and λ are model-dependent parameters. Later on we will discuss the determination of these parameters in the electroweak theory. The generic graph of pressure versus temperature is similar to that for the strong interactions, that we discussed earlier. The pressures p_1 and p_2 of the low- and high-temperature phases become equal at the critical temperature T_c. Also shown as dashed lines are possible curves of superheating of the low-temperature phase to a maximum possible temperature T^+, and possible supercooling of the high-temperature phase to a minimum possible temperature T_0. Origins of T^+ and T_0 are shown in Fig. 12, which displays the likely behaviour of the effective potential as the temperature is increased. The zero-temperature potential has a well-defined global minimum at $\chi \neq 0$. At the temperature T_0, the curvature of the effective potential at the origin changes from being negative (the low-temperature case) to positive (the high-temperature case). It is only above this temperature

that the $\chi = 0$ minimum of the effective potential is metastable, so T_0 represents the minimum possible supercooling temperature. At T_c, the minima at $\chi \neq 0$ and at $\chi = 0$ have equal heights, corresponding to the critical temperature. At T^+, the local minimum at $\chi \neq 0$ and the local maximum between there and $\chi = 0$ merge giving a point of inflexion. Above this temperature, there is not even a metastable minimum with $\chi \neq 0$, so this represents the maximum possible superheating temperature. It is easy to calculate T^+, T_0 and T_c in the effective potential model of Eq. (2.39) . One finds

$$T_0 = T_c\sqrt{1 - \frac{2}{9}\,\frac{\alpha^2}{\lambda\gamma}} \qquad T^+ = T_0/\sqrt{1 - \frac{1}{4}\,\frac{\alpha^2}{\lambda\gamma}} \tag{2.40}$$

The effective potential for the electroweak Higgs boson has been calculated in successive approximations: tree-level, one-loop, daisies, superdaisies, illustrated in Fig. 13. We relate the calculations to the Landau mean-field expansion shown in Eq. (2.39), using as inputs the Standard Model parameters, principally m_H. To keep things simple, we will start working with a pure $SU(2)$ theory, i.e., take the limit $g' = 0$. The one-loop calculations in this approximate theory yield [23]

$$\begin{aligned}
\alpha &= \frac{3}{16\pi}\,g^3 \simeq \frac{1}{18\pi} \\
\lambda &= \frac{g^3 m_H^2}{8 m_W^2} \simeq \left(\frac{m_H}{342\ \mathrm{GeV}}\right)^2 \\
\gamma &= \frac{3}{16}\,g^2 + \frac{\lambda}{2} \simeq \frac{1}{12} + \frac{1}{2}\left(\frac{m_H}{342\ \mathrm{GeV}}\right)^2 \\
T_0 &= \frac{m_H}{\sqrt{2\gamma}} \simeq m_H\sqrt{6}
\end{aligned} \tag{2.41}$$

for the Landau mean-field expansion parameters, where we have shown approximate numerical values for $g \simeq 2/3$ as in the Standard Model . Now that we have these potential parameters, it is an easy matter to calculate quantities of interest concerning the nature of the electroweak phase transition

$$\begin{aligned}
1 - \frac{T_0^2}{T_c^2} &= \frac{2}{9}\,\frac{\alpha^2}{\lambda\gamma} \simeq \left(\frac{10\ \mathrm{GeV}}{m_H}\right)^2 \ll 1 \\
\frac{v(T_c)}{v} &= \sqrt{\frac{4}{9}\,\frac{\alpha^2}{\lambda\gamma}}\,\frac{T_c}{T_0} \simeq \left(\frac{14\ \mathrm{GeV}}{m_H}\right) \ll 1 \\
\frac{L}{T_c^4} &= \frac{4}{9}\,\frac{\alpha^2\gamma}{\lambda^3}\,\frac{T_0^2}{T_c^2} \simeq \left(\frac{20\ \mathrm{GeV}}{m_H}\right)^4 \ll 1 \\
\frac{v(T_c)}{T_c} &= \frac{2}{3}\,\frac{\alpha}{\lambda} \simeq \left(\frac{37\ \mathrm{GeV}}{m_H}\right)^2 \ll 1
\end{aligned} \tag{2.42}$$

The fact that all these quantities are much smaller than unity for physical values of the Higgs boson mass (we recall that direct searches at LEP force $m_H > 65$ GeV, as discussed in Lecture I) means that the electroweak phase transition is weakly first-order in this approximation. Note also that the scalar field correlation length, corresponding to the Compton wave-length and hence range of the Higgs field

$$\xi_H(T_c) = \frac{1}{m_H(T_c)} = \frac{3}{\sqrt{2}}\,\frac{\sqrt{\lambda}}{\alpha}\,\frac{1}{T_c} \simeq \frac{1}{10\ \mathrm{GeV}} \simeq 0.02\ \mathrm{fm} \tag{2.43}$$

is almost independent of m_H and T_c, and quite large by electroweak standards. Its large size also indicates that, although first-order, the electroweak transition may be "close" to being second order. The penetration depth corresponding to the range of the gauge field

$$\xi_W(T_c) = \frac{1}{m_W(T_c)} = \frac{2}{gv(T_c)} \simeq \left(\frac{m_H}{21\ \mathrm{GeV}}\right)^2 \frac{1}{T_c} \gg \frac{1}{T_c} \tag{2.44}$$

is also large at the critical temperature.

The first step beyond this one-loop approximation is to include daisy diagrams (see Fig. 13c), which give [24]

$$\begin{aligned} \delta m_H^2 &= \frac{1}{4}\left(\frac{3}{4}g^2 + h_t^2\right)T^2 \\ \delta m_{W_L}^2 &= \frac{11}{6}g^2T^2 \\ \delta m_{W_T}^2 &= 0 \end{aligned} \tag{2.45}$$

where h_t denotes the Yukawa coupling of the top quark. From this we see that the Higgs and the longitudinal W have now acquired Debye screening masses, and are hence no longer in a position to contribute to α. Note, however, that the transverse W's still have zero mass and hence contribute to α. The fact that the H and W_L no longer contribute to α means that the strength of the first-order transition is reduced by about 2/3

$$T_c = 97\ \mathrm{GeV}\ ,\quad v(T_c) \simeq 40\ \mathrm{GeV} \tag{2.46}$$

The next step is to calculate the superdaisy diagrams (see Fig. 13d), which yield [25]

$$\delta m_{W_T} = \frac{g^2T}{3\pi} \tag{2.47}$$

However, this result is not reliable, because perturbation theory is not applicable to calculating the magnetic mass of a gauge boson. The normal assumption at this stage is a parametrisation

$$\delta m_{W_T} = \tau\,\frac{g^2T}{3\pi} \tag{2.48}$$

where τ is a parameter that is essentially non-perturbative. Studies show that the transition would become second-order if $\tau \gtrsim 2$.

This is as far as one can get with perturbation theory, and to get any further one needs a non-perturbative technique such as the lattice. Shown below are typical results of a high-temperature three-dimensional lattice simulation [26] of a pure $SU(2)$ electroweak theory:

m_H(GeV)	$\frac{v(T_c)}{T_c}\Big\|_{1-\mathrm{loop}}$	$\frac{v(T_c)}{T_c}\Big\|_{\mathrm{lattice}}$
35	1.1	1.1 to 2.0
80	0.2	0.7 to 0.9

(2.49)

These results and others indicate that the electroweak phase transition may be more strongly first order than suggested by the previous perturbative calculations. If so, the origin is likely to be different from that in perturbation theory [27]. It remains to be seen whether these initial lattice calculations are reliable, and for the moment we take the view that the weight of evidence is that the electroweak phase transition is weakly first order, although probably not so weak as the QCD phase transition discussed in Section 2.3.

3. Supersymmetry and Grand Unification

3.1. Why supersymmetry?

The motivation for supersymmetry that I find most compelling is the hierarchy/naturalness problem [28]. The general requirement of "naturalness" is that quantum corrections "should" be not much larger than their physical values. This requirement is respected by the quantum corrections to the mass of an elementary fermion such as the electron

$$\delta m_f \simeq m_f \left(\frac{\alpha}{\pi}\right) \ln\left(\frac{\Lambda}{m_f}\right) \tag{3.1}$$

Although formally infinite, as reflected in the logarithmic dependence on the cut-off Λ, this quantum correction is $\lesssim m_f$ for all values of the cut-off $\Lambda \lesssim m_P$. Many physicists consider that naturalness is a "reasonable" request for a "sensible" physical theory, but it is a requirement that goes beyond the pure mathematics of renormalisation. The mechanics of renormalisation theory, that is used to extract calculable results from field theory, does not care about the relative magnitudes of quantum corrections and physical values. However, if a quantum correction δX is much larger than the physical value of some quantity X_0, this means that the bare value must have been chosen in just such a way as to produce a large cancellation of the quantum correction

$$X = X_0 + \delta X \; : \; |X| \ll |X_0| \, , \; |\delta X| \tag{3.2}$$

which looks unnatural. It must be admitted, however, that naturalness is a subjective criterion that is in the mind of the beholder.

Naturalness is a problem for an elementary Higgs boson, as in the electroweak sector of the Standard Model , because it must have a mass in the range [29]

$$m_W = 0\left(\sqrt{\frac{\alpha}{\pi}}\right)^{0\pm1} \times m_H \tag{3.3}$$

The reason why this is a problem is that quantum corrections like those in Fig. 14a are quadratically divergent and hence very large if the cut-off $\Lambda \gg 1$ TeV

$$\delta m_H^2 \simeq g_{f,W,H}^2 \int^{\Lambda} \frac{d^4k}{(2\pi)^4} \; \frac{1}{k^2} \simeq 0\left(\frac{\alpha}{\pi}\right) \Lambda^2 \gg m_H^2 \tag{3.4}$$

For example, if $\Lambda \sim m_P$ or m_{GUT}.

The hierarchy problem is why $m_W \ll m_P(m_{GUT})$. An alternative way of formulating this question is to ask why is $G_F \gg G_N$? Equivalently, one can ask why the Coulomb potential between electron and nucleus is much greater than the Newton gravitational potential

$$V_{\rm Coulomb} = \frac{e^2}{r} \gg V_{\rm Newton} = \frac{G_N m^2}{r} \simeq \left(\frac{m_W^2}{m_P^2}\right)\frac{1}{r} \tag{3.5}$$

One difficulty is to know why $m_W \ll m_P$ in some initial approximation, say the classical tree-level approximation, and the other difficulty is to understand how such a hierarchy can be maintained despite the depredations of the quantum corrections shown in Eq. (3.4). The danger is that they will drive $m_H \to m_P$, unless there is very clever fine-tuning of the parameters, and carry along m_W as suggested by Eq.(3.3).

Another aspect of this problem arises in theories with both large and small scales. There tends to be "leakage" of the large scale which pollutes the small scale [30]. For example, in a GUT there is almost inevitably a coupling λ between electroweak Higgses with a small v.e.v. v and Higgses with a large GUT v.e.v. V. Such a coupling as shown in Fig. 14b would give rise to a correction

$$\delta m_H^2 \simeq \lambda V_{GUT}^2 \tag{3.6}$$

to the "light" Higgs boson mass. Even if $\lambda = 0$ at the tree level (do not ask me why, that is the hierarchy problem), non-zero couplings are in general regenerated [31] by quantum corrections of the type shown in Fig. 14c

$$\delta m_H^2 \simeq 0\left(\frac{\alpha}{\pi}\right)^2 V_{GUT}^2 \tag{3.7}$$

What one needs is a symmetry which suppresses not only λ but also all these quantum corrections through many, many orders of perturbation theory. As if this is were not enough, Hawking [32] has argued that a generic theory of quantum gravity will induce large corrections

$$\delta m_H^2 = 0(m_P^2) \tag{3.8}$$

To be sure of this assertion, one needs a consistent quantum theory of gravity, and the only one available is string theory. As it is difficult if not impossible to formulate a consistent, stable string theory without invoking supersymmetry, so let us now explore supersymmetry in more detail.

Supersymmetry works many miracles, for example in the loop diagrams shown in Fig. 14a. When I said a while back that each of these diagrams was quadratically divergent, I neglected to tell you that the fermion and boson diagrams had opposite signs, as a result of the difference between Fermi-Dirac and Bose-Einstein statistics

$$\delta m_{W,H}^2 \simeq -\left(\frac{g_F^2}{4\pi^2}\right)\left(\Lambda^2 + m_F^2\right) + \left(\frac{g_B^2}{4\pi^2}\right)\left(\Lambda^2 + m_B^2\right) \tag{3.9}$$

We see immediately that the quadratic divergences cancel if the couplings $g_F = g_B$ for pairs of bosons and fermions. Moreover, the residual corrections proportional to m_F^2 and m_B^2 would be small if $m_B \simeq m_F$. Equal couplings and almost equal masses mean approximate supersymmetry. Assuming this, we extract from Eq. (3.9)

$$\delta m_{W,H}^2 \simeq 0\left(\frac{\alpha}{\pi}\right) |m_B^2 - m_F^2| \tag{3.10}$$

which is $\lesssim m_{W,H}^2$, in agreement with the physical requirement of naturalness, if

$$|m_B^2 - m_F^2| \lesssim 1 \text{ TeV}^2 \tag{3.11}$$

Historically, this was the first physical motivation for low-energy supersymmetry [33]. However, *it must be emphasized again that this argument is a qualitative, physical argument that must* be regarded a matter of taste: an unnatural theory is still mathematically renormalizable, and hence acceptable to some people.

In addition to the above miracle, many logarithmic divergences are absent in supersymmetric theories [34]. Indeed, one finds that

$$\delta\lambda \propto \lambda \tag{3.12}$$

which vanishes if $\lambda = 0$. (Please do not ask me why $\lambda = 0$, that is again the hierarchy problem.) This means that if $\lambda = 0$ at the tree level, it vanishes to all orders of perturbation theory. As a result if these two miracles, if $m_W \ll m_P$ at the tree level, supersymmetry guarantees that it stays small through all orders of perturbation theory.

3.2. Model-building

The first question to ask when constructing a supersymmetric model is whether any of the known matter fermions q, ℓ can be related to any of the known bosons γ, W, Z, H, g. Unfortunately, model-builders soon realised that this was impossible. For example, quarks q occur in 3 representations of colour, whereas bosons only appear in 1 (γ, W, Z, H) or 8 (g) representations of the *colour group. Similarly, leptons carry a conserved lepton number* $L = 1$, *whereas all the known* bosons have zero lepton number. In particular, if one tried to associate a lepton with a Higgs boson in a supermultiplet

$$\begin{pmatrix} \ell \\ H \end{pmatrix} \tag{3.13}$$

then the theory would have an uncontrollably large amount of lepton number violation [35]. For this reason, we are forced to introduce superpartners for all the known particles, as shown in Table 2. You may be appalled by the proliferation of new particles, but remember that this trick has served particle physicists well in the past. They have repeatedly found that introducing new particles was the only way out of their dilemmas. Remember the invention of the ν to rescue

Table 2.1: Particles and Sparticles

Particle	Spin	Spartner	Spin
quark: q	$\frac{1}{2}$	squark: $\tilde{q}$	0
lepton: ℓ	$\frac{1}{2}$	slepton: $\tilde{\ell}$	0
photon: γ	1	photino: $\tilde{\gamma}$	$\frac{1}{2}$
W	1	wino: $\tilde{W}$	$\frac{1}{2}$
Z	1	sino: $\tilde{Z}$	$\frac{1}{2}$
Higgs: H	0	higgsino: $\tilde{H}$	$\frac{1}{2}$

energy conservation in β-decay, the invention of the $W^{\pm}$ and Z^0 to make a sensible theory of the weak interactions, and the introduction of charm to suppress unwanted neutral current interactions. Even if supersymmetry is not economical in particles, it is economical in principles!

Most supersymmetric theories contain one stable particle which should have been produced in the early Universe, and should be around today as a cosmological relic from the Big Bang [36]. This particle exists because most supersymmetric theories have a multiplicatively conserved quantum number called R parity [35], which takes the value +1 for all known particles, and -1 for all sparticles. It is easy to check using the forms of interaction given in the previous section that R parity is conserved by all the usual interaction vertices

$$f\bar{f}\tilde{G}\ ,\quad f\tilde{f}\tilde{H}\ ,\quad |\tilde{f}^2|^2\ ,\quad |\tilde{f}H|^2\ ,\quad \ldots \tag{3.14}$$

The conservation of R parity is not mysterious, since it is linked to the conservation of baryon number B and lepton number L. Indeed, one can represent R parity by

$$R = (-1)^{3B+L+2S} \tag{3.15}$$

where S is the spin. This equation immediately tells us how it would be possible to violate R parity conservation, namely by breaking B and/or L in an appropriate way. This could be done in *vacuo* by a v.e.v. for some sneutrino field $\tilde{\nu}$, or by introducing a coupling between H and L supermultiplets. Both of these possibilities are constrained by laboratory limits on $\Delta L \neq 0$ interactions, and also by the cosmological constraints mentioned at the end of Lecture 4, but R violation cannot be completely excluded.

If we nevertheless assume R conservation, as occurs in most phenomenological models, we can draw three important conclusions.

1. Sparticles must always be produced in pairs, for example

$$e^+e^- \to \tilde{\mu}^+\tilde{\mu}^- \ , \quad \bar{p}p \to \tilde{q}\tilde{g}X \tag{3.16}$$

2. Heavier sparticles can only decay into final states containing lighter sparticles, for example

$$\tilde{e} \to e\tilde{\gamma} \ , \quad \tilde{q} \to q\tilde{g} \ , \quad \tilde{g} \to q\bar{q}\tilde{\gamma} \ , \quad \cdots \tag{3.17}$$

3. The lightest supersymmetric particle (LSP) is absolutely stable, since it has no available legal decay mode. It is this particle which is a candidate to be the supersymmetric relic from the Big Bang [36], discussed in more detail in Part IV.

3.3. Grand unification

The simplest GUT model is based on the group SU(5) [37], [31], for which the 15 fermion helicity states of each generation

$$(ude\nu_e) \ , \quad (cs\mu\nu_\mu) \ , \quad (tbr\nu_\tau) \tag{3.18}$$

are each assigned to reducible $\bar{5}$ and 10 representations of $SU(5)$

$$\bar{5} = \begin{pmatrix} d_1^c \\ d_2^c \\ d_3^c \\ \cdots \\ -e^- \\ \nu_e \end{pmatrix} \qquad 10 = \frac{1}{\sqrt{2}} \begin{pmatrix} 0 & u_3^c & -u_2^c & \vdots & u_1 & d_1 \\ -u_3^c & 0 & u_1^c & \vdots & u_2 & d_2 \\ u_2^c & -u_1^c & 0 & \vdots & u_3 & d_3 \\ \cdots & \cdots & \cdots & \cdots & \cdots & \cdots \\ -u_1 & -u_2 & -u_3 & \vdots & 0 & e^c \\ -d_1 & -d_2 & -d_3 & \vdots & -e^c & 0 \end{pmatrix} \tag{3.19}$$

Note that colour $SU(3)$ acts on the first three indices, weak $SU(2)$ on the last two indices, and the $U(1)$ of hypercharge is a diagonal generator of the group. The gauge bosons are represented by

$$24 = \begin{pmatrix} & & & \vdots & X_1 & Y_1 \\ & g_{1\ldots8} & & \vdots & X_2 & Y_2 \\ & & & \vdots & X_3 & Y_3 \\ \cdots & \cdots & \cdots & \cdots & \cdots & \cdots \\ \bar{X}_1 & \bar{X}_2 & \bar{X}_3 & \vdots & W & \\ \bar{Y}_1 & \bar{Y}_2 & \bar{Y}_3 & \vdots & & \end{pmatrix} \tag{3.20}$$

Symmetry breaking in $SU(5)$ is achieved via two sets of Higgs bosons, one of which yields the first stage of GUT symmetry breaking

$$SU(5) \to SU(3)_C \times SU(2)_L \times U(1)_Y \tag{3.21}$$

for which we need, at least, an adjoint 24 Higgs representation ϕ

$$24 \quad \phi \; : \quad \langle 0|\phi|0\rangle = V \begin{pmatrix} 1 & & & & \\ & 1 & & 0 & \\ & & 1 & & \\ & 0 & & -\frac{3}{2} & \\ & & & & -\frac{3}{2} \end{pmatrix} \tag{3.22}$$

The second stage of symmetry breaking

$$SU(2)_L \times U(1)_Y \to U(1)_{em} \tag{3.23}$$

is achieved by a 5 Higgs representation H

$$5 \quad H \; : \quad \langle 0|H|0\rangle = \begin{pmatrix} 0 \\ 0 \\ 0 \\ . \\ 0 \\ 1 \end{pmatrix} v \tag{3.24}$$

which contains the doublet Higgs present in the Standard Model . The fermion assignments in the $SU(5)$ GUT are unique. The only place to put the colour singlet, $SU(2)$ doublet (ν, e) is in the $\bar{5}$ representation, and for the total charge in that representation to be zero, one must put the three colours of d^c. As for the 10, it contains a (1, 1) of $SU(3) \times SU(2)$ which is suitable for the e^c, a $(3, 2)$ that is suitable for the (u, d) doublet, and the remaining places are taken by the three colours of u^c. It is remarkable how simply and elegantly the quarks and leptons fit into this simplest GUT group.

The biggest apparent obstacle to Grand Unification is the inequality of the Standard Model gauge couplings

$$g_3 \gg g_2, g_1 \tag{3.25}$$

After all, the strong interactions are strong, and the weak weak, at present-day energies. This problem is resolved [38] by the logarithmic variations of g_3, g_2 and g_1, as exemplified by the asymptotic freedom of the strong coupling

$$\alpha_3(Q) \simeq \frac{12\pi}{(33 - 2N_q)\ln Q^2/\Lambda^2} + \ldots \tag{3.26}$$

discussed in Lecture I. We recall that in this leading-order formula, N_q stands for the number of light quarks, Q is the energy scale at which the coupling is measured, and Λ is the scale where the strong interactions become strong, which has an experimental value

$$\Lambda = 200 \text{ MeV} \times 2^{0\pm1} \tag{3.27}$$

The decrease Eq. (3.26) of the strong coupling, not forgetting the logarithmic variation of α_2 also, allows the possibility that $\alpha_3 = \alpha_2$ at some mass energy scale m_X. This can be seen most conveniently in terms of the inverses of the gauge couplings

$$\frac{1}{\alpha_3(Q^2)} - \frac{1}{\alpha_2(Q^2)} = \frac{11 + N_H/2}{12\pi} \ln \frac{Q^2}{m_X^2} + \dots \tag{3.28}$$

where N_H is the number of electroweak Higgs doublets, and the dots represent higher-order terms. Note that when $Q = m_X$, the first term on the right-hand side vanishes, and $\alpha_3(m_X) = \alpha_2(m_X)$. We also see from Eq. (3.28) that m_X must be exponentially high, because of the relatively slow logarithmic variation of the couplings. Indeed, since $\alpha_3 \simeq 1$ and $\alpha_2 \simeq \alpha_{em}$ in the neighbourhood of the strong interaction scale Λ, we find

$$\frac{m_X}{\Lambda} = \exp\left(\frac{0(1)}{\alpha_{em}} + 0(\ln \alpha_{em}) + 0(1) + \dots\right) \tag{3.29}$$

The hypothesis of grand unification can be used to predict $\sin^2\theta_W$. The variations of couplings with energy Q are determined by renormalisation group equations, which take the following form through two-loop order

$$Q\,\frac{\partial \alpha_i(Q)}{\partial Q} = -\frac{1}{2\pi}\left(b_i + \frac{b_{ij}}{4\pi}\,\alpha_j(Q)\right)\left[\alpha_i(Q)\right]^2 + \dots$$

$$b_i = \begin{pmatrix} 0 \\ -22/3 \\ -11 \end{pmatrix} + N_g \begin{pmatrix} 4/3 \\ 4/3 \\ 4/3 \end{pmatrix} + N_H \begin{pmatrix} 1/10 \\ 1/6 \\ 0 \end{pmatrix} \tag{3.30a}$$

$$b_{ij} = \begin{pmatrix} 0 & 0 & 0 \\ 0 & -136/3 & 0 \\ 0 & 0 & -102 \end{pmatrix} + N_g \begin{pmatrix} 19/5 & 3/5 & 44/15 \\ 1/5 & 49/3 & 4 \\ 4/30 & 3/2 & 76/3 \end{pmatrix} + N_H \begin{pmatrix} 9/50 & 9/10 & 0 \\ 3/10 & 13/6 & 0 \\ 0 & 0 & 0 \end{pmatrix} \tag{3.30b}$$

where the one-loop coefficients are given in (3.30a) and the two-loop coefficients in (3.30b). Note that in each of Eq. (3.30a) and Eq. (3.30b), the first terms are those associated with the gauge multiplets, the second are those associated with matter particles in $N_g = 3$ fermion generations, and the last terms are due to the Higgs fields, with N_H denoting the number of Higgs doublets. The renormalisation coefficients are independent of the specific GUT model, and are due entirely to the conventional Standard Model particles.

One can use experimental values of α_{em} and α_3, together with the hypothesis that $\alpha_3 = \alpha_2 = \alpha_1$ at m_X to predict [39]

$$\sin^2\theta_W(m_Z)_{\overline{\rm MS}} = 0.208 + 0.004(N_H - 1) + 0.006 \ln\left(\frac{400\ \text{MeV}}{\Lambda_{\overline{\rm MS}}\ (N_f = 4)}\right) \tag{3.31}$$

which yields

$$\sin^2\theta_W(m_Z)_{\overline{\rm MS}} = 0.214 \pm 0.002 \tag{3.32}$$

if $N_H = 1$ and Λ =100 - 200 MeV, to be contrasted with the latest LEP value [9]

$$\sin^2\theta_W(m_Z)_{\overline{\rm MS}} = 0.2324 \pm 0.0006 \tag{3.33}$$

Here, $\overline{MS}$ denotes a specific prescription for calculating higher-order diagrams. Can one resolve this discrepancy in a non-supersymmetric model? The answer is not by adding in more matter generations, which do not contribute to Eq. (3.31). You could get a better value of $\sin^2\theta_W$ by adding in more Higgs doublets, but this would simultaneously decrease the value of m_X and cause the proton lifetime to be catastrophically short. The discrepancy cannot be removed by varying m_t or α_3 within experimentally-allowed ranges. Another way of stating the discrepancy between Eqs. (3.31) and (3.33) is that if one uses the experimental value Eq. (3.33) for $\sin^2\theta_W$ together with the experimental values of α_{em} and α_3, the extrapolated gauge couplings do not all become equal at a single energy [40], as seen in Fig. 15a.

The most economical way of resolving all these discrepancies and problems is to postulate low-energy supersymmetry [41]. In this case, the renormalization coefficients in Eq. (3.30) are modified as follows: at one loop

$$b_i = \begin{pmatrix} 0 \\ -6 \\ -9 \end{pmatrix} + N_g \begin{pmatrix} 2 \\ 2 \\ 2 \end{pmatrix} + N_H \begin{pmatrix} 3/10 \\ \frac{1}{2} \\ 0 \end{pmatrix} \tag{3.34a}$$

and two loops

$$b_{ij} = \begin{pmatrix} 0 & 0 & 0 \\ 0 & -24 & 0 \\ 0 & 0 & -54 \end{pmatrix} + N_g \begin{pmatrix} \frac{38}{15} & \frac{6}{5} & \frac{88}{15} \\ \frac{2}{5} & 14 & 8 \\ \frac{11}{5} & 3 & \frac{68}{3} \end{pmatrix} + N_H \begin{pmatrix} \frac{9}{50} & \frac{9}{10} & 0 \\ \frac{3}{10} & 7/2 & 0 \\ 0 & 0 & 0 \end{pmatrix} \tag{3.34b}$$

where the coefficients are - again - independent of the specific GUT, as long as it incorporates supersymmetry. The gauge couplings measured at low energies appear to agree better with the predictions of a supersymmetric GUT [40], and Fig. 15b shows that the couplings measured at low energies extrapolated to high energies using Eqs. (3.34) are consistent with all being equal at the supersymmetric grand unification scale. However, it is not possible [42] yet to use this agreement to deduce the values of the supersymmetric particle masses, as shown in Fig. 15c. As one varies α_3 over the allowed range from 0.110 to 0.130, one can accomodate any value of the supersymmetry-breaking gaugino mass $m_{1/2}$ between 10 GeV and many orders of magnitude above the expected 1 TeV scale. This type of analysis of the gauge couplings is *consistent* with supersymmetric GUT unification, but does not *prove* it, nor *fix* the supersymmetry-breaking scale.

3.4. Neutrino masses, mixing and oscillations

Neutrino masses are much smaller than those of the corresponding leptons and quarks [43]

$$\begin{aligned} m_{\nu_e} &\lesssim 7.2 \text{ eV} \\ m_{\nu_\mu} &\lesssim 270 \text{ keV} \\ m_{\nu_\tau} &\lesssim 24 \text{ MeV} \end{aligned} \tag{3.34}$$

while the limit on m_{ν_e} comes from studies of the end-point in Tritium β-decay, the upper limit on m_{ν_μ} comes from studies of $\pi \to \mu\nu$ decay, and the upper limit on m_{ν_τ} comes from the end-point of $\tau \to \nu_\tau 5\pi$. The second distinctive feature of neutrinos is that only left-handed neutrinos have ever been observed in the laboratory. In the Standard Model , this is because only left-handed neutrinos appear in the electroweak charge current

$$J_\mu = \bar{e}\gamma_\mu(1-\gamma_5)\nu_e + \bar{\mu}\gamma_\mu(1-\gamma_5)\nu_\mu + \bar{\tau}\gamma_\mu(1-\gamma_5)\nu_\tau \tag{3.35}$$

Neither the Standard Model nor the minimal $SU(5)$ GUT contain right-handed neutrinos, whilst both quarks q and leptons ℓ have both left- and right-handed states. This means that quarks and charged leptons can have "Dirac" masses

$$g_{Hff}\, H_{\substack{\Delta I=1/2\\ \Delta L=0}}\ \ \bar{f}_R f_L \Rightarrow m_f^D = g_{Hff}\ \langle 0|H_{\substack{\Delta I=1/2\\ \Delta L=0}}|0\rangle \tag{3.36}$$

generated by a v.e.v. for the Standard Model Higgs boson with $\Delta I = 1/2, \Delta L = 0$. A puzzle then arises: if ν_R exists, why are the m_ν so much smaller than $m_{q,\ell}$? If the ν_R do not exist, can m_ν be non-zero?

The answer to the second question is affirmative, because one can replace the $\bar{f}_R$ in Eq. (3.36) by f_L^c. Thus there is a "Majorana" neutrino mass term

$$m^m \nu_L^T C \nu_L = m^m \bar{\nu}_L^c \nu_L \equiv m^m\, "\nu_L \nu_L" \tag{3.37}$$

which does not exist for either quarks or charged leptons. If we tried to couple two q^L fields together, we would have $\Delta Q_{em}, \Delta C \neq 0$, and if we tried to couple to ℓ_L together we would have $\Delta Q_{em} \neq 0$, which are not possible for mass terms. Note, however, that the Majorana mass term in Eq. (3.37) requires lepton number violation $\Delta L = 2$ and weak isospin $\Delta I = 1$. There is no Higgs field with such quantum numbers in either the Standard Model or minimal $SU(5)$. However, such a Majorana mass term

$$\tilde{g}_{H\bar{\nu}\nu}\, H_{\substack{\Delta I=1\\ \Delta L=2}}\ \ "\nu_L \nu_L" \Rightarrow m^M = \tilde{g}_{H\bar{\nu}\nu}\ \langle 0|H_{\substack{\Delta I=1\\ \Delta L=2}}|0\rangle \tag{3.38}$$

is possible and present in some more complicated GUT models Higgs fields, or could appear via higher-order non-renormalizable couplings [44] such as

$$\frac{1}{M}\ \ (H_{\Delta I=1/2}\nu_L)\ \ (H_{\Delta I=1/2}\nu_L) \tag{3.39}$$

Here M is a heavy mass parameter which could originate from the exchange of a massive ν_R

$$\frac{1}{M} = \frac{g^2}{M_{\nu_R}} \tag{3.40}$$

This mass could in turn arise from a Majorana mass term with $\Delta I = 0$.

Combining all the possible sources of neutrino masses discussed in the previous paragraph, we arrive at the following generic "see-saw" neutrino mass matrix [45]

$$(\nu_L\ ,\ \ \bar{\nu}_R)\ \begin{pmatrix} m^M & m^D \\ m^D & M^M \end{pmatrix}\ \begin{pmatrix} \nu_L \\ \bar{\nu}_R \end{pmatrix} \tag{3.41}$$

where m^M is a $\Delta I = 1$ Majorana mass, m^D is a Dirac mass which is $\cong m_{q/\ell}$ in many GUT models, and M^M is a $\Delta I = 0$ Majorana mass term. Generically, we expect in GUTs that

$$m_{\nu_e} \ll m_{\nu_\mu} \ll m_{\nu_\tau} \tag{3.42}$$

See, for example the $\mathbf{5}$ of $SU(5)$ with $\Delta I = 1/2$, and the $\mathbf{24}$ of $SU(5)$ with $\Delta I = 0$. Diagonalising the mass matrix in Eq. (3.41), we obtain the following mass eigenstates, where M should be understood as lying anywhere in the range $m_P \gtrsim M \gtrsim (\alpha/\pi)^2 \times m_X$

$$\begin{aligned} \nu_L + 0\left(\frac{m_W}{M}\right)\bar{\nu}_R \quad &: \quad m = 0\left(\frac{m_W^2}{M}\right) \\ \nu_R + 0\left(\frac{m_W}{M}\right)\bar{\nu}_L \quad &: \quad m = 0(M) \end{aligned} \tag{3.43}$$

If we extend the above picture to three generations, neglect possible neutrino mixing, and assume that the large Majorana masses M_i do not depend strongly on the generation index i, we arrive at the following likely hierarchy of light neutrino masses

$$m_{\nu_i} \sim \frac{m_{l_i}^2 \text{ or } m_{q_i}^2}{M_i} \Rightarrow m_{\nu_e} \ll m_{\nu_\mu} \ll m_{\nu_\tau} \tag{3.44}$$

In this picture, the most likely candidate to constitute Hot Dark Matter would be the ν_τ, which could have a mass around 10 eV if $M_3 \sim 10^{12}$ GeV.

In point of fact, we do expect the different flavours of neutrinos to mix analogously to the quarks leading to neutrino oscillations [46]. Experiments searching for low-energy solar neutrinos ($E_\nu \lesssim 10$ MeV) see fewer than expected in the standard solar model. The explanation for this apparent deficit could be partly experimental and partly astrophysical. However, one favoured explanation is that the neutrinos produced by the sun mix and oscillate before reaching the Earth. The most likely neutrino oscillation scenario seems to be matter-enhanced mass oscillations of neutrinos within the Sun [47]. According to this hypothesis, Fig. 16 shows the preferred regions of the $(\sin^2\theta,\ \Delta m^2)$ plane [48]. According to the generic GUT see-saw neutrino mass matrix shown in Eq. (3.41), the most likely hypothesis would be $\nu_e \to \nu_\mu$ oscillations, with

$$\sin^2\theta_{e\mu} \simeq 10^{-2} \tag{3.45}$$

If one scales up [49] the resulting $m_{\nu_\mu} \sim 3 \times 10^{-3}$ eV with the expected hierarchical ratio

$$m_\nu \sim m_u^2 \quad : \quad m_c^2 \quad : \quad m_t^2 \tag{3.46}$$

one easily finds $m_{\nu_\tau} \cong 10$ eV, which would be just right for the ν_τ to constitute Hot Dark Matter with $\Omega_\nu \cong 0.3$, as suggested by models [50] of structure formation in the aftermath of COBE [51]. Moreover, one is led [49] to the likelihood that

$$\sin^2\theta_{\mu\tau} \sim 10^{-3} \text{ to } 10^{-4} \tag{3.47}$$

which is within reach of a new round of neutrino oscillation experiments currently under preparation at CERN [52].

3.5. Sphalerons and leptogenesis

Much of the interest in the electroweak phase transition has been triggered by the discovery that the electroweak interactions violate baryon and lepton number non-perturbatively [12], and the possibility that this might provide scenarios for cosmological baryogenesis, if the electroweak phase transition were sufficiently strongly first order. In this section, I will try to give you some idea of the reasons how and why non-perturbative electroweak effects violate B and L. The first fact to recognise is that the vacuum structure in a gauge theory is very complicated, with many configurations whose energies are equal in perturbation theory, as seen in Fig. 17. The horisontal axis is labelled by the so-called Chern-Simons number. The perturbative effects discussed up to now correspond to analysing small quantum fluctuations in the gauge and Higgs fields A_μ, ϕ around one of these vacua. Non-perturbative effects include transitions between different vacua labelled by different values of the Chern-Simons number. In a pure (unbroken) gauge theory such as QCD, these transitions are generated by instantons [12], which are configurations of the gauge field A_μ

$$A_\mu \; : \; \frac{g^2}{32\pi^2} \int d^3\mathrm{x} \; F_{\mu\nu} \tilde{F}^{\mu\nu} = N_I \; : \; \tilde{F}^{\mu\nu} \equiv \epsilon^{\mu\nu\rho\sigma} F_{\rho\sigma} \tag{3.48}$$

where N_I is an integer. Things are more complicated in the electroweak theory, which possesses classical non-perturbative field configurations of (A_μ, ϕ) called sphalerons [53], that correspond to bumps in the effective potential shown in Fig. 17. These are unstable saddle points of the effective potential, which have masses

$$E_{sph} \simeq \frac{m_W(T)}{\alpha} \simeq 10 \text{ TeV} \tag{3.49}$$

These two classes of non-perturbative configuration mediate transitions with rates

$$e^{-4\pi/\alpha_W} \; , \; e^{-\beta E_{sph}} \approx e^{-\frac{m_W(T)}{\alpha_W T}} \tag{3.50}$$

The instantons at $T = 0$ are negligible, but the sphalerons at $T \neq 0$ can be very important [54]. Remember that $m_W(T) \to 0$ at high temperatures, so the exponential suppression vector vanishes.

The next point to recognise is that these non-perturbative transitions between vacua with different Chern-Simons number violate baryon number B and lepton number L, since these non-perturbative gauge field configurations contribute to the divergences of the corresponding baryon and lepton number currents

$$\partial^\mu J^{baryon}_\mu = N_g \left[\frac{g^2}{32\pi^2} \int d^3\mathrm{x} F_{\mu\nu} F^{\mu\nu} = \partial^\mu J^{lepton}_\mu \right] \tag{3.51}$$

Here N_g is the number of matter generations, known from LEP to be three, and the factor in square brackets is an integer $N = 1, 2, \ldots$. The corresponding changes in B and L are

$$\Delta B = N_g = 3 = \Delta L \tag{3.52}$$

Note that although B and L are violated, the combination $(B-L)$ is conserved. The rate of baryon number violation is given by

$$(B+L) = -c(B+L)\,T\exp\,(-\frac{E_{sph}}{T}) \tag{3.53}$$

in the low-temperature phase where the electroweak gauge symmetry is broken. As already mentioned, the exponential suppression factor tends to vanish at high temperatures, and it is expected that in the high-temperature symmetric phase

$$E_{sph}(T) \simeq \frac{m_W(T)}{\alpha_W} \to 0 \tag{3.54}$$

where c is a numerical coefficient that can only be estimated using non-perturbative techniques [55]. Lattice simulations of theories thought to be analogous to gauge theory indicate that

$$(B+L) = -c(B+L)T \tag{3.55}$$

Comparing the rate of $(B+L)$ violation with the Hubble expansion rate, we see that baryon and lepton number violating processes were presumably in equilibrium at temperatures above the electroweak critical temperature, implying that

$$(B+L) = 0 \tag{3.56}$$

This point should be taken into account in any scenario for cosmological baryogenesis.

Let us recall the three Sakharov [56] conditions for cosmological baryogenesis

1. Interactions that violate baryon number

   These are present non-perturbatively in the Standard Model , thanks to the sphalerons discussed in the previous section.

2. Interactions that distinguish matter and antimatter

   This means interactions that violate the following discrete symmetries. Charge conjugation C changes particles into antiparticles and vice versa

   $$f \leftrightarrow \bar{f}(f^c) \tag{3.57}$$

   The combination of charge conjugation with parity P, denoted CP, exchanges particles and antiparticles and simultaneously exchanges left with right

   $$(\overleftarrow{f} + \overrightarrow{f}) \leftrightarrow (\overrightarrow{\bar{f}} + \overleftarrow{\bar{f}^c}) \tag{3.58}$$

   It has been known for a long time that the charged-current weak interactions violate C maximally. The violation of CP has been seen in a laboratory in the weak decays of kaons. In particular,

   $$P(K \to \pi^+ e^- \nu) \neq P(K \to \pi^- e^+ \bar{\nu}) \tag{3.59}$$

this result is interpreted as evidence for CP violation in the mass matrix mixing K_0 and $\bar{K}_0$.

3. Interactions that are out of thermal equilibrium

   Thermodynamics in the form of Boltzmann's H-theorem tells us that the population of states in equilibrium depends only on their mass, and it is a sacred theorem of quantum field theory that particles and antiparticles have identical masses. Therefore, thermal equilibrium forbids any matter-antimatter asymmetry.

The non-perturbative electroweak baryon number violating interactions described in the previous section would wash out rapidly any previously-generated $(B+L)$ asymmetry, , and hence tend to wash out any baryon asymmetry generated by GUTs, for example. However, if the GUT were able to generate a $(B-L)$ asymmetry, this would survive the electroweak sphaleron wash-out. Alternatively, one could try to generate the baryon asymmetry via the electroweak interactions, which would be possible if the electroweak phase transition were sufficiently strongly first order, so that sphaleron interactions were out of equilibrium below the electroweak critical temperature, as discussed above. A third possibility would be to use the equilibrium sphalerons at high temperatures to reprocess a pre-existing lepton asymmetry [57]. This works as follows: if there is an initial net lepton number $L_i \neq 0$, then the $(B+L)$-violating sphalerons ensure that

$$B_f + L_f = 0 \tag{3.60}$$

However, $B-L$ conservation ensures that

$$B_f - L_f = -L_i \tag{3.61}$$

The solution of these last two equations is to generate

$$B_f = -\frac{L_i}{2} \tag{3.62}$$

An example of such a scenario will now be given.

The suggestion [57] is that heavy neutrinos ν^c could have decayed out of equilibrium, their dominant decays being $\nu^c \to (\nu, \ell)H$ via a Dirac mass coupling. Higher-order diagrams could cause C and CP violation in ν^c decays, leading to a lepton asymmetry

$$\epsilon_1 = \frac{1}{2\pi(\lambda_L^\dagger \lambda_L)_{ii}} \sum \mathrm{Im}\ \left[(\lambda_L^\dagger \lambda_L)_{ij}\right]^2 f\left(\frac{m_j^2}{m_i^2}\right) \tag{3.63}$$

Subsequent reprocessing by electroweak sphalerons, which violate $(B+L)$ but conserve $(B-L)$, could turn this lepton asymmetry into a baryon asymmetry. For this mechanism to work, one needs

$$m_{\nu^c} < m_{inflaton} \lesssim 10^{13}\ \mathrm{GeV} \tag{3.64}$$

which is consistent with the above fit to the solar neutrino problem and the suggestion that the ν_τ could constitute the Hodt Dark Matter in the Universe.

4. Dark Matter

4.1. Running hot and cold dark matter?

Inflation tells us to expect that the density of the Universe as a whole is indistinguishable from the critical density: $\Omega = 1$. However, observations only provide $\Omega_{visible} \lesssim 0.01$, whereas Big Bang nucleosynthesis apparently restricts $\Omega_B \lesssim 0.1$. Measurements of rotation curves suggest that galactic haloes contain $\Omega_{halo} \sim 0.1$. Thus the halo could in principle be made out of baryons, although arguments have been given that these could not be in the form of gas, dust or snowballs. However, the possibility that they could be "Jupiters" or brown dwarfs, i.e., small, "failed" stars remains open. Some microlensing events caused by brown dwarfs have apparently been seen [58]. However, it is not clear whether they are due to objects in the galactic halo, or in the galactic disc, or the Large Magellanic Cloud. It still seems likely that there is a substantial contribution to the local halo density, estimated to be

$$\rho_{halo} \sim 0.3\,\mathrm{GeV\,cm^{-3}} \sim 0.01\,m_\odot\,pc^{-3} \tag{4.1}$$

from non-baryonic dark matter.

Theories of galaxy formation seem to require some non-baryonic dark matter to enhance initial density perturbations via gravitational instability. Theorists of structure formation in the early Universe distinguish two categories of dark matter: hot, which was relativistic when galaxy-sized perturbations came within the event horison and began to grow, and cold, which was non-relativistic at that epoch. The one you favour depends on your pet theory of galaxy formation. If you believe these formed from a Gaussian random field of perturbations laid down during inflation, then you should prefer cold dark matter. This is because it enables perturbations to grow on all scales from galaxies upwards, whereas hot dark matter escapes from small galaxy-sized perturbations, retarding their growth. Thus, in a pure hot dark matter scenario, galaxies only form late as a result of larger structures breaking up. This scenario seemed to be disfavoured by the observation of galaxies and quasars at high redshifts, as well as by other considerations. However, if galaxies formed from seeds, such as cosmic strings, hot dark matter might be preferred.

Assuming some type of inflationary scenario, the comparison of COBE [51] and other large-scale data with other data on structures at smaller scales seems to require a modification of the pure cold dark matter scenario. One possibility is that there is a non-zero cosmological constant, but this seems very unlikely from the point of view of particle physics, since there is no known natural reason why the cosmological constant should be in the range of cosmological utility. The two prime candidates for modifying the standard cold dark matter scenario seem to be a mixed dark matter with an admixture of hot dark matter

$$\Omega_{Cold} \sim 0.7,\ \Omega_{Hot} \sim 0.3,\ \Omega_{Baryons} \lesssim 0.1 \tag{4.2}$$

or a tilt in the spectrum of primordial density perturbations. The parameters of these two models can be fixed by galaxies and by the COBE data, which fix the overall normalisation of $\delta\rho/\rho$: the question is then what the models predict at intermediate scales, in particular for the peculiar motions of clusters. At least some astrophysicists will tell you that the cold dark matter with tilt model predicts peculiar motions on the scale of clusters that are too small by comparison with

the data. Moreover, at least in simple models one expects very small amount of tilt. Therefore, my own preference at the moment is for a mixed dark matter model as in Eq. (4.2).

4.2. Massive neutrinos

Figure 18 shows a sketch of the relic "neutrino" density, or the density of some other neutral particle coupled to the Z^0, as a function of its possible mass. When the neutrino mass is very small (less than 1 MeV), the relic neutrino number density is independent of the mass, and hence the relic energy density

$$\rho_\nu \propto m_\nu \tag{4.3}$$

When the mass of the neutrino increases above about 30 eV, this neutrino density exceeds the critical density, and we enter a disallowed range of neutrino masses. We emerge from this disallowed region again when the neutrino mass is of order a few GeV [59], when the number density of neutrinos is suppressed by a Boltzmann factor $e^{-m_\nu/T}$. Since the neutrino energy density is inversely proportional to the $\bar{\nu}\nu$ annihilation cross-section, as we shall see in more detail in the next paragraph, the relic neutrino density is very small for neutrinos ing about $m_Z/2$, whilst the relic neutrino density increases again for larger values of m_ν. We are therefore left with three interesting ranges of neutrino masses

$$m_\nu \sim 30 \text{ eV} \ , \quad m_\nu \sim 3 \text{ GeV} \ , \quad m_\nu \sim 1 \text{ TeV} \tag{4.4}$$

Neutrinos would constitute Hot Dark Matter in the first window, and Cold Dark Matter in either of the second or third windows. I know of no well-motivated alternatives to neutrinos as Hot Dark Matter, but there are other candidate Cold Dark Matter particles whose relic abundance is calculated in a similar way to that of neutrinos.

The density of massive relic particles in a generic particle physics model may be estimated as follows [59]. It is controlled by the annihilation rate

$$\frac{dn}{dt} = -3\,\frac{\dot{a}}{a}\,n - \langle\sigma_{ann}v\rangle\,(n^2 - n_0^2) \tag{4.5}$$

where n is the particle number density, the first term on the right-hand side is the normal dilution due to the Hubble expansion, the last term is due to annihilation with a relative velocity v, and n_0 denotes the normal Bose-Einstein or Fermi-Dirac equilibrium number density. In most cases of interest, one can expand the low-energy annihilation cross-section in the general form

$$\langle\sigma_{ann}v\rangle \simeq a + bx \ : \quad x \equiv \frac{\langle v^2\rangle}{6} \tag{4.6}$$

There is a simple approximate solution for $n(t)$, called the freeze-out approximation. According to this, $n = n_0$ until

$$\dot{n}_0 \simeq \langle\sigma_{ann}v\rangle n_0^2 \tag{4.7}$$

which occurs at a characteristic temperature, that of freeze-out T_f. Thereafter, the evolution of the number density is supposed to be given by

$$\dot{n} \simeq \langle \sigma_{ann} v \rangle n^2 \tag{4.8}$$

Exact numerical calculations for a number of particle candidates confirm that this freeze-out approximation give results which are accurate to about 20 % in most cases, yielding

$$\rho \simeq 0.8 \, (T_\chi)^3 \, \frac{m_\chi}{a x_f + 1/2 b x_f^2} \tag{4.9}$$

where the first factor on the right-hand side is a correction for the naïve freeze-out approximation, and T_χ is the effective temperature of the relic particles, which is related to that of photons ($T_\gamma \simeq 2.73K$) by the number of effective degrees of freedom at the freeze-out temperature T_f

$$\left(\frac{T_\chi}{T_\gamma} \right)^3 \simeq \left(\frac{g_{eff}(T_f)}{g_{eff}(\text{low } E)} \right)^{-3/4} \tag{4.10}$$

One can represent the relic density as

$$\rho \simeq 4.0 \times 10^{-40} \, \left(\frac{T_\chi}{2.8^0 k} \right)^3 \, g_{eff}^{1/2} \, \left(\frac{\text{GeV}^{-2}}{a x_f + 1/2 b x_f^2} \right) \, g \text{ cm}^{-3} \tag{4.11}$$

in convenient units.

4.3. Lightest supersymmetric particle

We saw in Lecture III that in many supersymmetric theories the lightest supersymmetric particle or LSP is likely to be absolutely stable and hence a good candidate for a cosmological relic from the Big Bang [36]. The LSP is likely to be electromagnetically neutral and have only weak interactions with baryonic matter, and the possible candidates are: sneutrinos $\tilde{\nu}$ of spin 0, some gaugino/Higgsino mixture called generically a neutralino χ of spin 1/2, and the gravitino $\tilde{G}$ of spin 3/2. We will now discuss which of these candidates appears to be the most plausible.

Sneutrino $\tilde{\nu}$

Such a Cold Dark Matter particle would have coherent spin-independent interactions with heavy nuclei, which have not been seen in underground experiments using Si and Ge materials [60], yielding the constraints

$$m_{\tilde{\nu}} \lesssim 10 \text{ GeV} \quad \text{or} \quad \gtrsim 1 - 10 \text{ TeV} \tag{4.12}$$

The first inequality can be strengthened by considering possible sneutrino capture by the Sun, followed by annihilation with the production of high-energy neutrinos from the solar core. The

fact that these have not been seen tells us that $\tilde{\nu}$ escape from the Sun, and hence must be light [61]

$$m_{\tilde{\nu}_{e,\mu}} \lesssim 4 \text{ GeV} \tag{4.13}$$

Finally, as was pointed out in the previous section, the LEP neutrino counting experiments tell us that

$$m_{\tilde{\nu}} \gtrsim 40 \text{ GeV} \tag{4.14}$$

Combining these constraints we see that the $\tilde{\nu}$ is ruled out as the Cold Dark Matter particle unless it weighs more than 1-10 TeV, in which case it is unlikely to be the lightest supersymmetric particle.

Gravitino $\tilde{G}$

In the absence of cosmological inflation, the relic number density of gravitinos would be somewhat smaller than that of photons or neutrinos, since gravitinos would have decoupled from the Universe at a very early epoch [62]. This means that the gravitino mass required to give the critical density is about

$$m_{\tilde{G}} \sim 1 \text{ keV} \tag{4.15}$$

Such neutrinos would constitute "Warm" rather than Hot or Cold Dark Matter. If there was a cosmological inflationary epoch, the primordial density of gravitinos would be suppressed, and the above limit does not apply. Indeed, models suggest that

$$m_{\tilde{G}} \gtrsim m_s > 45 \text{ GeV} \tag{4.16}$$

in which case the gravitino would not be the lightest supersymmetric particle, and again the limit in Eq. (4.16) does not apply. In view of Eq. (4.16), the possibility that the gravitino is the LSP appears implausible, but it cannot be ruled out. We can only hope that the gravitino is indeed not the LSP, because its interactions with ordinary matter are so weak that it is unlikely it could ever be detected.

Neutralino χ

This is a generic name for a mixture of neutral spin-1/2 gauginos and higgsinos $\tilde{\gamma}/\tilde{Z}/\tilde{H}_1/\tilde{H}_2$, which is parametrised by the unmixed gaugino mass $m_{1/2}$, the Higgs mixing parameter μ, and $\tan\beta = v_2/v_1$, the ratio of Higgs v.e.v.'s in the MSSM. The full mass matrix for neutral gauginos and higgsinos is [36]

$$M_{\tilde{N}} = \begin{pmatrix} M_2 & 0 & \frac{-g'v_1}{2} & \frac{g'v_2}{2} \\ 0 & M_1 & \frac{gv_1}{2} & \frac{-gv_2}{2} \\ \frac{-g'v_1}{2} & \frac{gv_1}{2} & 0 & \mu \\ \frac{g'v_2}{2} & \frac{-gv_2}{2} & \mu & 0 \end{pmatrix} \tag{4.17}$$

The lightest mass eigenstate, which is the best candidate to be the LSP and hence Cold Dark Matter [36], simplifies in the limits $m_{1/2} \to 0$, in which case it is approximately a photino $\tilde{\gamma}$, and $\mu \to 0$, in which case it is a higgsino $\tilde{H}$. However, a generic LSP is a complicated mixture, as you can well imagine from the matrix in Eq. (4.17). Figure 19 shows the domains of parameter space allowed by searches at LEP and other accelerators for the LSP and other related supersymmetric particles. They tell us that [63]

$$m_\chi \gtrsim 10 \text{ to } 20 \text{ GeV} \tag{4.18}$$

The constraints used in drawing Fig. 19 include that from the invisible Z^0 decay width (neutrino counting), the total Z^0 decay width, the peak Z^0 peak cross-section, searches for $Z \to \chi\chi'$ followed by $\chi' \to \chi(\ldots)$ decays, called zen events, unsuccessful searches for charged partners of the neutralinos, and the unsuccessful search for gluinos at the FNAL $\bar{p}p$ collider. Also shown in Fig. 18 are regions of parameter space where an "interesting" amount of Cold Dark Matter can be found, namely

$$\Omega h^2 = 0.1 \text{ to } 1 \tag{4.19}$$

for some values of the other supersymmetric model parameters.

We conclude that the spin-1/2 neutralino χ is a very good candidate to be the Cold Dark Matter beloved of astrophysicists, and we will devote the rest of this lecture to discussing strategies for experimental searches for this LSP.

4.4. Searches for cold dark matter particles

Annihilations in the galactic halo

Here the basic idea [64] is that massive Cold Dark Matter particles, such as the neutralinos discussed in Lecture 8, will occasionally meet in the galactic halo, annihilating into l^+l^- or $\bar{q}q$ pairs for the most part, which can then lead to stable particles such as antiprotons, positrons, photons or neutrinos in the cosmic rays. All such stable particles fluxes share the same dependences setcounterequation0

$$\phi_{\bar{p},e^+,\gamma} \propto n^2 \sigma_{\text{Ann}} \tau \tag{4.20}$$

on the local halo density of Cold Dark Matter particles n, corresponding to the expected halo density of around 0.3 GeV cm^{-3}, on the relic annihilation cross-section σ_{Ann}, and on the length of time that the produced particle spends within the galaxy. In my view [65], the best way to fix the annihilation cross-section is to assume that the Cold Dark Matter particle has the closure density. The corrections in a mixed dark matter model, in which $\Omega_{cold} \simeq 0.7$, would not be very different, and are easy to take into account[1]. A much larger source of uncertainty is the time τ that the produced particle spends in the galaxy. This is easy to calculate in the case of a photon

[1] If there is an admixture of Hot Dark Matter neutrinos: $\Omega_{hot} \simeq 0.3$, these are not expected [66] to constitute a large fraction of the galactic halo.

or neutrino, being given simply by the light travel time from the annihilation point, but is rather uncertain in the case of $\bar{p}$'s and e^+'s. The other factors in Eq. (4.20) have to be estimated from dynamical models of the differential distribution dn/dE expected from a given $\bar{f}f$ annihilation final state. The best guide [67] to the latter may be a Monte Carlo program of the type developed to model final-state particle spectra in e^+e^- annihilation at LEP and elsewhere.

The first stable annihilation product to be considered was the $\bar{p}$, particularly at low energies. The flux of $\bar{p}$'s at moderate energies above about 1 GeV is qualitatively consistent with cosmic-ray models assuming the secondary production of $\bar{p}$ by primary matter cosmic-ray particles. At one time, it was claimed that there might be an excess of low-energy $\bar{p}$'s with a typical energy around 200 MeV [68]. However, this apparent anomaly disappeared, and the present low-energy data [69] are also qualitatively consistent with the normal matter cosmic-ray model. The methods outlined in the previous paragraph can be used to derive from these experiments an upper bound on a number density of massive Cold Dark Matter relic particles, in particular on the number density of neutrinos. The cosmic ray e^+ flux can also be used to derive upper limits on the neutralino number density. Both of these limits are sensitive to the assumed time that the $\bar{p}$'s and e^+'s spend in a galactic magnetic field.

Typical upper limits [65] on the neutralino density from $\bar{p}$ and e^+ fluxes are shown in Fig. 20. We see that the $\bar{p}$'s give slightly more stringent upper limits, and conclude that

$$\rho_{\tilde{\gamma},A} \lesssim (5 \text{ to } 10) \times \rho_{\text{Halo}} \tag{4.21}$$

is the conservative upper limit from these cosmic-ray studies. Since the stable particle fluxes depend quadratically on the neutralino density, as seen in Eq. (4.20), and the confinement time of antiprotons and positrons in the galactic magnetic field is rather uncertain, it seems to me unlikely that searches for these particles will give us useful information about the neutralino halo density.

Annihilations in the Sun or Earth

Here the basic idea is as follows. As a relic particle in a galactic halo passes through the solar system, it may pass through the Sun [70] (or Earth [71]) itself, and perhaps undergo there an elastic collision with one of the nuclei (mainly protons) beneath the solar surface. Such a collision would cause the relic particle to lose energy to the struck nucleus, and this energy loss might convert it from an initially hyperbolic orbit into an elliptic orbit with a perihelion below the solar surface. Then it would pass repeatedly through the Sun, losing more energy through collisions with nuclei inside the Sun from time to time, until eventually it settled into an approximately isothermal distribution, characterized by energy balance with the solar nuclei. It has been proposed [72] that such a process might actually cause the core of the Sun to cool, by transferring thermal energy to outer regions of the Sun. This would be of interest for low-energy solar neutrinos, since it would tend to reduce their calculated flux. Detailed calculations indicate, however, that this is not possible with supersymmetric particles. The population of relic particles within the Sun is controlled by annihilation and/or by evaporation [73], the particle analogues of civil war and emigration. Annihilations into $\bar{f}f$ final states could lead directly or indirectly to high-energy neutrinos detectable on Earth. Other annihilation products would of course be absorbed within the Sun. The high-energy neutrinos could be detected either directly in deep underground proton

decay experiments, or indirectly via upward-going muons produced by neutrino collisions in the rock beneath the detector.

As in the case of annihilations in the galactic halo, one finds [74] that with conservative and reasonable assumptions, one can at best establish an upper limit

$$\begin{aligned} \rho_{\tilde{\gamma}} &\lesssim 10 \times \rho_{\rm Halo} \quad \text{for} \quad m_{\tilde{\gamma}} \lesssim 10 \text{ GeV} \\ \rho_{\tilde{h}} &\lesssim 10 \times \rho_{\rm Halo} \quad \text{for} \quad m_{\tilde{h}} \lesssim 20 \text{ GeV} \end{aligned} \tag{4.22}$$

no range of m_{χ} is yet excluded at a level of the expected halo density, if one assumes that the neutralino relic density is close to the closure dentity. You may sometimes see parts of the $(\mu, m_{1/2})$ plane that are apparently excluded by searches for high-energy solar neutrinos [75], but so far these are regions where the relic neutrino density is any case much below the closure density, and probably unable to constitute the galactic halo.

Before leaving this method of searching for dark matter particles, it is worth commenting that matter-enhanced neutrino oscillations could conceivably cloud the interpretation of the experiments [76]. This is because even high-energy neutrinos produced in the core of the Sun may oscillate into other, less detectable, neutrino flavours before they reach the Earth. This effect is shown in Fig. 21 for a particular choice of oscillation parameters

$$\begin{aligned} \sin^2 2\theta &= 0.6 \\ \Delta m^2 &= 8 \times 10^{-6} \text{ eV}^2 \end{aligned} \tag{4.23}$$

that is consistent with the low-energy solar neutrino experiments. Here we see that the ν_e flux produced in the Sun is enhanced before arriving at the Earth, whilst the $\nu_{\mu,\tau}$ fluxes are relatively suppressed. It is also possible to find neutrino mass and mixing parameters such that the ν_e flux is suppressed, whilst the $\nu_{\mu,\tau}$ flux is enhanced. This possibility of neutrino flavour transmutation means that care must be exercised in interpreting upper limits from terrestrial searches for high-energy solar neutrinos. To be on the safe side, one should always assume [76] that by the time the neutrinos arrive at the Earth they have the flavour for which your detector efficiency is the smallest, generally the ν_τ.

Another place to look for possible neutrino annihilations is in the core of the Earth [71], following trapping of the neutralinos there by a process similar to that in the Sun. Since the composition of the Earth is different from that of the Sun, the calculation of the trapping rate is different, and the trapping efficiency has a different dependence on the neutralino mass. First searches have been made for a high-energy neutrino flux emanating from the earth core, but these have also not yet attained the sensitivity required to see the galactic halo density of neutralinos.

Dark matter searches in the laboratory

Here the principal interest is in elastic scattering of Cold Dark Matter particles on heavy nuclei [77]. The typical recoil energy in such a collision is

$$\Delta E < m_\chi v^2 = 10 \left(\frac{m_\chi}{10 \text{ GeV}} \right) \text{ keV} \tag{4.24}$$

where we have assumed a typical galactic velocity $v \simeq 300$ km s^{-1}. The neutralino-nucleus scattering rate is built up in several steps, starting with the effective interaction Lagrangian between neutralinos and the quark constituents of a proton or neutron inside the nucleus. This takes the form

$$\mathcal{L}_{eff} = \sum_q [(\bar{\chi}\gamma_\mu\gamma_5\chi)\ (\bar{q}\gamma^\mu(A_q P_L + B_q P_R)q) + (\bar{\chi}\chi)\cdot C_q m_q \bar{q}q] \tag{4.25}$$

where $P_{L,R} \equiv 1/2(1 \pm \gamma_5)$, the first term is due to sfermion $\tilde{f}$ and Z_0 exchange and is spin-dependent, whilst the second term is due to $\tilde{f}$ and H exchange and is spin-independent.

The next step is to estimate the spin-dependent neutralino-nucleon scattering matrix elements, which may be written as

$$M_{SD}(\chi_{(p,n)} \to \chi_{(p,n)}) = 4\mathrm{S}_\chi \cdot \mathrm{S}_{(p,n)} \sum_{q\in(p,n)} (B_q - A_q)\,\Delta q \tag{4.26}$$

Initially, theorists used the naïve constituent quark model to estimate the Δq [77]. However, recent experiments at CERN and elsewhere [78] indicate that the naïve quark model does not give an adequate picture of the quark contributions to the proton and neutron spins. Instead, a better approximation seems to be given [79] by the Skyrme model, which treats protons and neutrons as rotating coherent clouds of very light u, d and s quarks. In what follows, we will assume [80] the following values for the quark contributions to the proton spin

$$\Delta u = 0.77 \pm 0.08\ ,\quad \Delta d = -0.49 \pm 0.08\ ,\quad \Delta s = -0.15 \pm 0.08 \tag{4.27}$$

which are extracted from the EMC experiment and close to the Skyrme model predictions. Recent experiments on polarised muon- and electron-neutron scattering give estimates of the Δq which are quite consistent with Eq. (4.27), but with smaller errors. For a recent review of experimental determinations of Δq, see Ref. [81].

The matrix element for the spin-independent part of the neutralino-nucleon scattering amplitude may be parametrised by [82]

$$M_{SI}\Big(\chi(p,n) \to \chi(p,n)\Big) = (\bar{\chi}\chi)\cdot(m_p\bar{p}p, m_n\bar{n}n)$$
$$\left[\hat{f}\,\frac{m_u C_u + m_d C_d}{m_u + m_d} + fC_s + \frac{2}{27}(1 - f - \hat{f})\,\Big(C_u + C_b + C_t\Big)\right] \tag{4.28}$$

Here $\hat{f} \simeq 0.05$ and $f \simeq 0.2$ have the interpretations of the fractions of the proton mass carried by $u + d$ and s quarks, respectively. These quantities are related to other experimental observables, in particular the cross-section for low-energy π-nucleon scattering. For a review of the relevant strong interaction uncertainties, see Ref. [83]. The coefficients A_q, B_q and C_q are given in [80] and references therein.

The next step is to apply the above scattering amplitudes in Eqs (4.26) and (4.28) to estimate the scattering amplitudes for neutralinos on heavy nuclei containing many protons and neutrons.

This yields [84],[80],[85] the following expression for the elastic scattering rate of an LSP on a nucleus

$$R = (R_{SD} + R_{SI})\, Y \left(\frac{4 m_\chi m_N}{(m_\chi + m_N)^2}\right) \left(\frac{\rho_\chi}{0.3 \text{ GeV cm}^{-3}}\right) \left(\frac{\langle |v_E| \rangle}{320 \text{ km s}^{-1}}\right) \text{ events kg}^{-1} \text{ day}^{-1} \quad (4.29)$$

where Y is the isotopic abundance of the nuclei considered, ρ_{LSP} is alocal halo density of LSPs, and v_E is the mean LSP velocity relative to the Earth. The first two terms in Eq. (4.29) are the spin-dependent and spin-independent expressions shown below

$$R_{SD} = 580\ \lambda^2 J(J+1)\ \zeta(r_{spin})\ \left(10^4 \text{ GeV}^2 \sum_q (B - A)\Delta q\right)^2 \quad (4.30)$$

where λ is given by one's nuclear model, $\zeta(r_{spin})$ is the spin form factor, and

$$R_{SI} = 210 m_N^2 m_Z^4\, \zeta(r_{charge}) \left(\hat{f}\, \frac{m_u C_u + m_d C_d}{m_u + m_d} + f C_s + \frac{2}{27}\,(1 - f - \hat{f})\,(C_c + C_b + C_t)\right)^2 \quad (4.31)$$

where $\zeta(r_{charge})$ is the Fermi mass form factor. To normalise the scattering rate, we adjust the sparticle parameters so that $\Omega_{LSP} = 1$ for $H_0 = 50$ km s^{-1} Mpc^{-1}.

Typical results [85] are shown in Fig. 22. Comparing Figs. 22a and 22b, we see that the scattering rates are dependent on the Higgs sector of the theory, parametrised here by the pseudoscalar Higgs mass m_A. In the case of Fluorine, the rate is dominated by the spin-dependent interaction. We see that, at least in the case $m_A = 200$ GeV, a large fraction of the $(\mu, m_{1/2})$ space in which $\Omega_{LSP} = 1$ is possible can be covered by realistic experiments. Figures 22c and 22d show the corresponding rates for a target containing equal amounts of ^{73}Ge and ^{76}Ge. In this case, the interaction is dominated by the spin-independent term, and there is little difference between the two isotopes of Germanium. We see that in this case, another large area of the $\Omega_{LSP} = 1$ space can be covered, and one which is somewhat complementary to that reachable using a Fluorine target. Finally, Figs. 22e and f show analogous rates for elastic scattering off Thallium, which seems to be the best choice if m_A is large. However, it should be emphasised that the elastic scattering rates for heavier nuclei are intrinsically less reliable. Figure 23 shows, for the combined Germanium target, the "probability" of LSP detection, defined to be the fraction of the parameter space where $\Omega_{LSP} = 1$ is possible for some choice of supersymmetric model parameters in which the elastic scattering rate is "observable", in the sense that the scattering rate exceeds 0.1 events kg^{-1}d^{-1}. We see that the elastic scattering experiment is likely to be successful if m_A is small, but is unlikely to be successful with this nucleus if m_A is very large. For comparison, Fig. 23 also shows the domains of this parameter space which can be explored using LEP and/or the LHC. We see that there is a fair amount of both redundancy and complementarity between the accelerator searches and the searches for Cold Dark Matter particles in the galactic halo.

Before leaving this subject, your attention is drawn to Ref. [86], in which inelastic LSP-nucleus scattering is considered. A priori, such a process is of experimental interest because it has a double signature, given by the combination of recoil energy and a de-excitation γ with an energy in the range 10-50 KeV, which might render the process observable at room temperature in a large detector. Unfortunately, as shown in Ref. [86], the rates found in a naïve shell model

are discouragingly low, only a few exceeding 10^{-4} kg^{-1}d^{1}. Therefore, I am unaware of any active experimental development programme to explore the inelastic scattering signature.

I conclude this lecture with the following Copernican challenge. Copernicus showed us that we were not at the centre of the Universe. Modern astrophysicists claim that we are not even made of the same stuff as most of the matter in the Universe. The challenge is to prove this latter assertion!

Bibliography

[1] S. Weinberg, "Gravitation and Cosmology" (Wiley, New York, 1972).

[2] E.W. Kolb and M.S. Turner, "The Early Universe" (Addison-Wesley, Redwood City, 1990).

[3] J. Ellis and G. Steigman, *Phys.Lett.* **89B** (1980) 186.

[4] C. Quigg, "Gauge Theories of the Strong, Weak and Electromagnetic Interactions" (Benjamin-Cummings, Reading, 1983).

[5] D. Ross and M. Veltman, *Nucl.Phys.* **B95** (1975) 135.

[6] E.S Abers and B.W. Lee, *Physics Reports* **9C** (1973) 1.

[7] M. Veltman, *Nucl.Phys.* **B123** (1977) 89.

[8] M.S. Chanowitz, M. Furman and I. Hinchliffe, *Phys.Lett.* **B78** (1978) 285.

[9] The LEP Collaborations ALEPH, DELPHI, L3 and OPAL, and the LEP Electroweak Working Group, CERN Report No. LEPEWWG/95-091;
P. Renton, rapporteur talk at Int. Symp. on Lepton and Photon Interactions at High Energies, Beijing 1995, Oxford preprint OUNP-95-20 (1995).

[10] J. Ellis, G.L. Fogli and E. Lisi, CERN preprint TH/95-202 (1995).

[11] C. Bouchiat, J. Iliopoulos and Ph. Meyer, *Phys.Lett.* **138B** (1972) 652 and references therein.

[12] G. 't Hooft, *Phys.Rev.* **D14** (1976) 3432;
R. Jackiw and C. Rebbi, *Phys.Rev.Lett.* **37** (1976) 172;
C.G. Callan, R.F. Dashen and D.J. Gross, *Phys.Lett.* **63B** (1976) 334.

[13] H.D. Politzer, *Phys.Rev.Lett.* **30** (1973) 1346;
D.J. Gross and F.A. Wilczek, *Phys.Rev.Lett.* **30** (1973) 1343.

[14] J. Gasser and H. Leutwyler, *Nucl.Phys.* **B250** (1985) 465.

[15] E. Witten, *Nucl.Phys.* **B223** (1983) 422,433;
G. Adkins, C.R. Nappi and E. Witten, *Nucl.Phys.* **B228** (1983) 552.

[16] A. Chodos et al., *Phys.Rev.* **D9** (1984) 3471.

[17] B.A. Campbell, J. Ellis and K.A. Olive, *Nucl.Phys.* **B345** (1990) 57.

[18] Y. Iwasaki et al., *Phys.Rev.* **D46** (1992) 4657;
B. Grossmann and M.L. Laursen, Jülich Preprint HLRZ-93-7 (1993);
Y. Iwasaki et al., CERN Preprint TH. 6798/93 (1993).

[19] J. Ignatius, K. Kajantie, H. Kurki-Suonio and M. Laine, *Phys.Rev.* **D49** (1994) 3854 and **D50** (1994) 3738.

[20] J.H. Applegate and C.J. Hogan, *Phys.Rev.* **D31** (1985) 3037;
J.H. Applegate, C.J. Hogan and R. Scherrer, *Phys.Rev.* **D35** (1987) 1151;
C. Alcock, G.M. Fuller and G.J. Mathews, *Ap.J.* **320** (1987) 439.

[21] D. Thomas, D.N. Schramm, K.A. Olive and B.D. Fields, *Ap.J.* **406** (1993) 569.

[22] A.D. Linde, *Nucl.Phys.* **B216** (1983) 421;
M. Dine et al., *Phys.Rev.* **D46** (1992) 550.

[23] G.W. Anderson and L.J. Hall, *Phys.Rev.* **D45** (1992) 2685.

[24] M.E. Carrington, *Phys.Rev.* **D45** (1992) 2933;
M. Dine et al., Ref. [45].

[25] J.R. Espinosa, M. Quirós and F. Zwirner, *Phys.Lett.* **B314** (1993) 206;
W. Buchmüller, Z. Fodor, T. Helbrig and D. Walliser, *Ann.Phys.* **234** (1994) 260.

[26] K. Kajantie, K. Rummukainen and M. Shaposhnikov, *Nucl.Phys.* **B407** (1993) 356.

[27] M. Shaposhnikov, CERN Preprint TH. 6918/93 (1993).

[28] G. 't Hooft, "Recent Developments in Field Theories", eds. G. 't Hooft et al. (Plenum Press, New York, 1980).

[29] M. Veltman, *Acta Phys.Pol.* **B8** (1977) 475;
C. Vayonakis, *Lett. Nuovo Cimento* **17** (1976) 383;
B.W. Lee, C. Quigg and H.B. Thacker, *Phys.Rev.* **D16** (1977) 1519.

[30] E. Gildener and S. Weinberg, *Phys.Rev.* **D13** (1976) 3333;
E. Gildener, *Phys.Rev.* **D14** (1976) 1667.

[31] A.J. Buras, J. Ellis, M.K. Gaillard and D.V. Nanopoulos, *Nucl.Phys.* **B135** (1978) 66.

[32] S. Hawking, D.N. Page and C. Pope, *Phys.Lett.* **86B** (1979) 175 and *Nucl.Phys.* **B170** (1980) 283.

[33] S. Dimopoulos and H. Georgi, *Nucl.Phys.* **B193** (1981) 150;
N. Sakai, *Z.Phys.* **C11** (1982) 153.

[34] J. Iliopoulos and B. Zumino, *Nucl.Phys.* **B76** (1974) 310;
S. Ferrara, J. Iliopoulos and B. Zumino, *Nucl.Phys.* **B77** (1974) 413.

[35] P. Fayet, *Phys.Lett.* **69B** (1977) 489 and **84B** (1979) 416.

[36] H. Goldberg, *Phys.Rev.Lett.* **50** (1983) 1419;
J. Ellis, J.S. Hagelin, D.V. Nanopoulos, K.A. Olive and M. Srednicki, *Nucl.Phys.* **B238** (1984) 453.

[37] H. Georgi and S.L. Glashow, *Phys.Rev.Lett.* **32** (1974) 438.

[38] H. Georgi, H. Quinn and S. Weinberg, *Phys.Rev.Lett.* **33** (1974) 451.

[39] W. Marciano and A. Sirlin, *Phys.Rev.Lett.* **46** (1981) 163.

[40] P. Langacker, University of Pennsylvania Preprint UPR 0238T (1990);
J. Ellis, S. Kelley and D.V. Nanopoulos, *Phys.Lett.* **B249** (1990) 441;
U. Amaldi, W. de Boer and H. Furstenau, *Phys.Lett.* **B260** (1991) 447.

[41] S. Dimopoulos and H. Georgi, Ref. [74];
S. Dimopoulos, S. Raby and F. Wilczek, *Phys.Rev.* **D24** (1981) 1681;
L. Ibáñes and G.G. Ross, *Phys.Lett.* **105B** (1981) 439.

[42] F. Anselmo, L. Cifarelli, A. Petermann and A. Zichichi, CERN Preprints PPE-91-123 (1991), TH. 6429/92 (1992), PPE-92-103 (1992);
J. Ellis, S. Kelley and D.V. Nanopoulos, *Nucl.Phys.* **B373** (1992) 55.

[43] Particle Data Group, K. Hikasa et al., *Phys.Rev.* **D50** (1994) 1173.

[44] R. Barbieri, J. Ellis and M.K. Gaillard, *Phys.Lett.* **90B** (1980) 249.

[45] T. Yanagida, Proc. Workshop on the Unified Theory and the Baryon Number in the Universe (KEK, Japan, 1979);
R. Slansky, Talk at the Sanibel Symposium, Caltech Preprint CALT-68-709 (1979).

[46] B. Pontecorvo, *Zh.Eksp.Teor.Fiz.* **33** (1957) 549; **34** (1958) 247; **53** (1967) 1717.

[47] L. Wolfenstein, *Phys.Rev.* **D17** (1978) 2369;
S.P. Mikheyev and A.Yu. Smirnov, *Nuovo Cimento* **9C** (1986) 17.

[48] P.I. Krastev and S.T. Petcov, *Phys.Lett.* **B299** (1993) 99.

[49] J. Ellis, J. Lopez and D.V. Nanopoulos, *Phys.Lett.* **B292** (1992) 189.

[50] See, e.g.: G. Efstathiou, J.R. Bond and S.D.M. White, *Mon.Not.R. Ast.Soc.* **258** (1992) 1P; and M.S. Turner, FNAL Preprint Conf-92/313-A (1992).

[51] G.F. Smoot et al., *Ap.J.Lett.* **396** (1992) L1;
E.L. Wright et al., *Ap.J.Lett.* **396** (1992) L13.

[52] CHORUS Collaboration, N. Armenise et al., CERN-SPSC/90-42 (1990);
NOMAD Collaboration, P. Astier et al., CERN-SPSC/91-21 (1991).

[53] F. Klinkhamer and N. Manton, *Phys.Rev.* **D30** (1984) 2212.

[54] V. Kuzmin, V. Rubakov and M. Shaposhnikov, *Phys.Lett.* **B155** (1985) 36.

[55] J. Ambjorn, T. Aksgaard, H. Porter and M. Shaposhnikov, *Nucl.Phys.* **B353** (1991) 346.

[56] A.D. Sakharov, *Pis'ma Zh.Eksp.Teor.Fiz.* **5** (1967) 32.

[57] M. Fukugita and T. Yanagida, *Phys.Lett.* **174B** (1986) 45.

[58] C. Alcock et al., *Nature* **365** (1993) 621;
E. Aubourg et al., *Nature* **365** (1993) 623.

[59] B.W. Lee and S. Weinberg, *Phys.Rev.Lett.* **39** (1977) 165;
P. Hut, *Phys.Lett.* **69B** (1977) 85.

[60] S.P. Ahlen et al., *Phys.Lett.* **B195** (1987) 603;
D.O. Caldwell et al., *Phys.Rev.Lett.* **61** (1988) 510;
F. Boehm et al., *Phys.Lett.* **B255** (1991) 143.

[61] J.S. Hagelin, K.W. Ng and K.A. Olive, *Phys.Lett.* **180B** (1986) 375.

[62] H. Pagels and J. Primack, *Phys.Rev.Lett.* **48** (1982) 223.

[63] L. Roszkowski, *Phys.Lett.* **B252** (1990) 471.

[64] J. Silk and M. Srednicki, *Phys.Rev.Lett.* **53** (1984) 624.

[65] J. Ellis et al., *Phys.Lett.* **B214** (1988) 403.

[66] J. Ellis and P. Sikivie, *Phys.Lett.* **B321** (1994) 390.

[67] S. Ritz and D. Seckel, *Nucl.Phys.* **B304** (1988) 877.

[68] A. Buffington, S.M. Schindler and C. Pennypacker, *Ap.J.* **248** (1981) 179.

[69] S.P. Ahlen et al., *Phys.Rev.Lett.* **61** (1988) 145;
T. Bowen et al., Arizona Preprint LHEA-89-006 (1989).

[70] J. Silk, K.A. Olive and M. Srednicki, *Nucl.Phys.* **B279** (1987) 804.

[71] A. Gould, *Ap.J.* **321** (1987) 571.

[72] G.B. Gelmini, L.J. Hall and M.J. Lin, *Nucl.Phys.* **B281** (1987) 726.

[73] A. Gould, *Ap.J.* **321** (1987) 560.

[74] J. Ellis, R.A. Flores and S. Ritz, *Phys.Lett.* **B198** (1987) 493.

[75] A. Bottino et al., Torino Preprint DFTT 33/92 (1992) and references therein;
M. Mori et al., *Phys.Lett.* **B270** (1991) 89.

[76] J. Ellis, R.A. Flores and S. Masood, *Nucl.Phys.* **B294** (1992) 229.

[77] M. Goodman and E. Witten, *Phys.Rev.* **D30** (1985) 3059.

[78] EMC Collaboration, J. Ashman et al., *Nucl.Phys.* **B328** (1989) 1.

[79] S.J. Brodsky, J. Ellis and M. Karliner, *Phys.Lett.* **B206** (1988) 309.

[80] J. Ellis and R.A. Flores, *Phys.Lett.* **B263** (1991) 259; *Nucl.Phys.* **B400** (1993) 25.

[81] J. Ellis and M. Karliner, *Phys.Lett.* **B313** (1993) 131.

[82] K. Griest, *Phys.Rev.* **D38** (1988) 2357, E, **D39** (1989) 3802.

[83] J. Gasser, H. Leutwyler and M.E. Sainio, *Phys.Lett.* **B253** (1991) 252.

[84] J. Ellis and R.A. Flores, *Nucl.Phys.* **B307** (1988) 883.

[85] J. Ellis and R.A. Flores, *Phys.Lett.* **B263** (1991) 259.

[86] J. Ellis, R.A. Flores and J.D. Lewin, *Phys.Lett.* **B212** (1988) 375.

FIGURE CAPTIONS

Fig. 1 The form of the Higgs potential in the electroweak theory.

Fig. 2 Tree diagrams contributing to $e^+e^- \to \bar{f}f$ at LEP.

Fig. 3 One-loop radiative corrections to the amplitudes for $e^+e^- \to \bar{f}f$, due to (a) vacuum polarization, (b) a vertex correction, and (c) a box diagram.

Fig. 4 One-loop contributions to the radiative correction Δr (1.44) due to the t quark and the Higgs boson, evaluated for $M_Z = 92$ GeV.

Fig. 5 The decrease with energy Q of the strong coupling as measured in many different experiments.

Fig. 6 Qualitative picture of the phase boundary between quark and hadron matter.

Fig. 7 Sketch of the phase transition proceeding (a) by tunnelling in the first-order case, (b) by rollover in the second-order case.

Fig. 8 (a) In a first-order transition, bubbles of the new vacuum form, whilst (b) in a second-order transition there is a spinodal decomposition into regions with different values of the order parameter.

Fig. 9 In a first-order transition, bubbles of the new vacuum are surrounded by a "cheese" made of the false vacuum. Bubbles smaller than the critical size r_b contract, whilst larger bubbles expand.

Fig. 10 Qualitative picture of the finite-temperature pressure curves in the hadron and quark phases of QCD.

Fig. 11 Constraints on inhomogeneous Big Bang nucleosynthesis models imposed by the observed light element abundances [21].

Fig. 12 The finite-temperature effective potential, showing its form at $T = 0$, $T = T_0$ when the symmetric vacuum becomes classically unstable, $T = T_c$ the usual critical temperature, and $T = T^+$ above which the asymmetric vacuum does not exist.

Fig. 13 Contributions to the effective potential (a) at the tree level, (b) at the one-loop level, (c) due to daisy diagrams, and (d) due to superdaisy diagrams.

Fig. 14 (a) Quadratically-divergent loop corrections to m_H^2, (b) a diagram which "leaks" the large mass-scale in a GUT into the light mass-scale, and (c) a quantum correction to this leakage.

Fig. 15 The low-energy couplings measured at LEP (a) do not extrapolate to grand unification without supersymmetry, but (b) do when supersymmetry is included [40], although (c) this agreement cannot be used to calculate reliably the supersymmetry-breaking scale [42].

Fig. 16 Matter-enhanced neutrino oscillation fits to the solar neutrino data [48].

Fig. 17 The effective potential in a spontaneously-broken gauge theory as a function of the Chern-Simons number.

Fig. 18 Qualitative picture of the neutrino relic density ρ_ν as a function of the neutrino mass m_ν.

Fig. 19 Regions of the $(\mu, m_{1/2})$ plane excluded by LEP and CDF searches, together with regions where the lightest neutralino mass $m_\chi < m_W$, and the relic neutralino density is in an "interesting" range $0.1 < \Omega_{LSP}h^2 < 1$.

Fig. 20 Upper limits on the photino or higgsino density in the galactic halo, from the absence of $\bar{p}$ or e^+ annihilation products [65].

Fig. 21 Possible matter-enhanced oscillation effects on the high-energy solar neutrino spectrum *due to relic annihilations* [76].

Fig. 22 Elastic scattering rates for (a), (b) ^{19}F, (c), (d) ^{73}Ge + ^{76}Ge, (e), (f), Tl, for the pseudoscalar Higgs mass $m_A = 70$ GeV in (a), (c), (e), 200 GeV in (b), (d), (f) [80], [85]. The rates are above 0.1 events $\mathrm{kg}^{-1}\mathrm{d}^{-1}$ in the shaded regions.

Fig. 23 The "probability" of detecting neutralino dark matter, as defined by the fraction of the parameter space where the critical density $\Omega_{LSP} = 1$ can be attained in which the χ-Ge elastic scattering rate exceeds 0.1 events $\mathrm{kg}^{-1}\mathrm{d}^{-1}$ [80], [85].

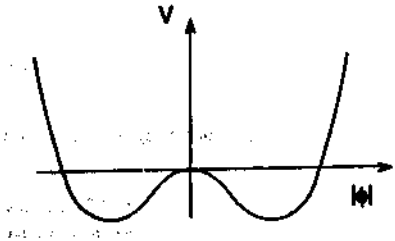

Fig. 1

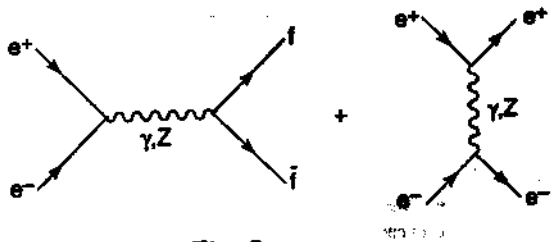

Fig. 2

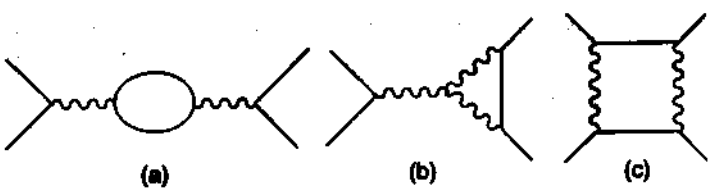

Fig. 3

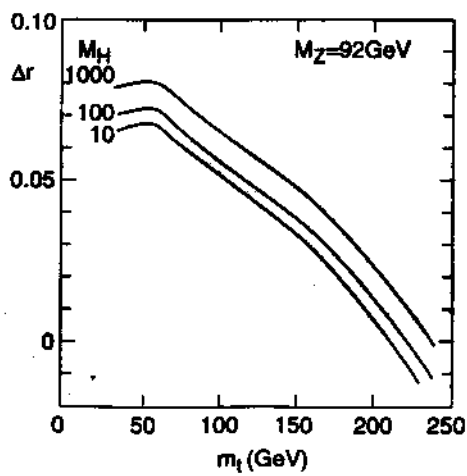

Fig. 4

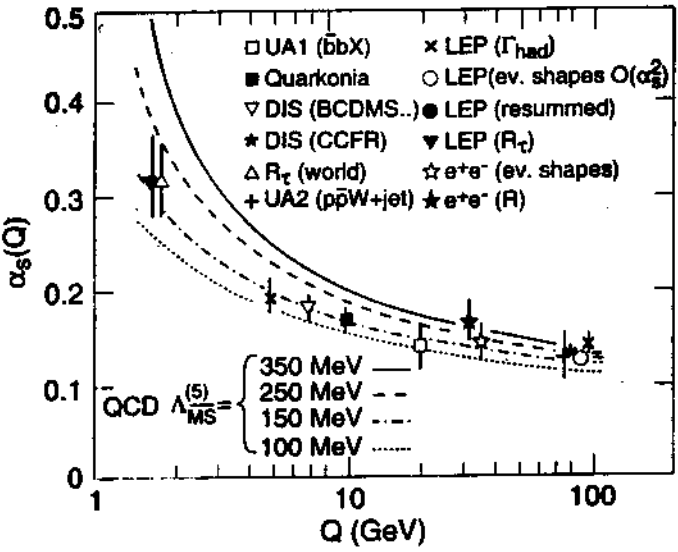

Fig. 5

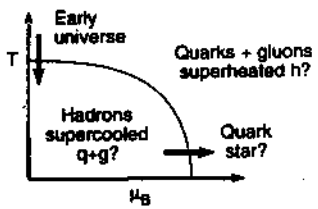

Fig. 6

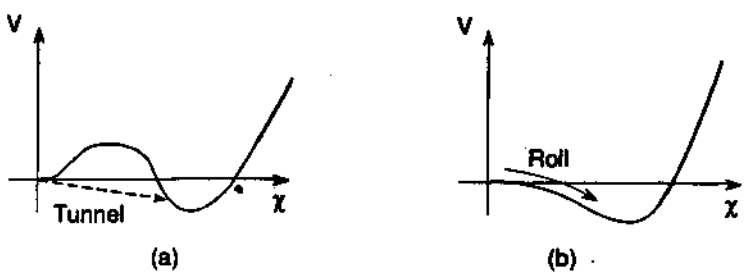

Fig. 7

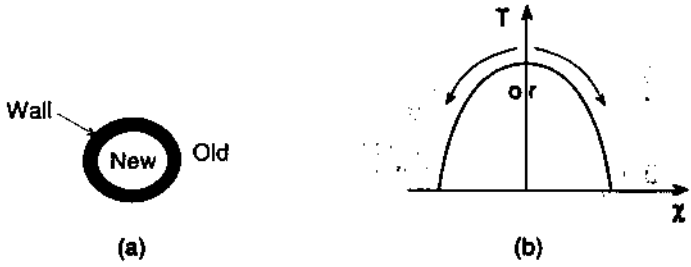

Fig. 8

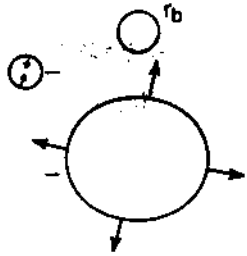

Fig. 9

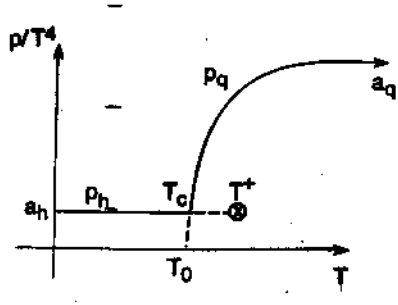

Fig. 10

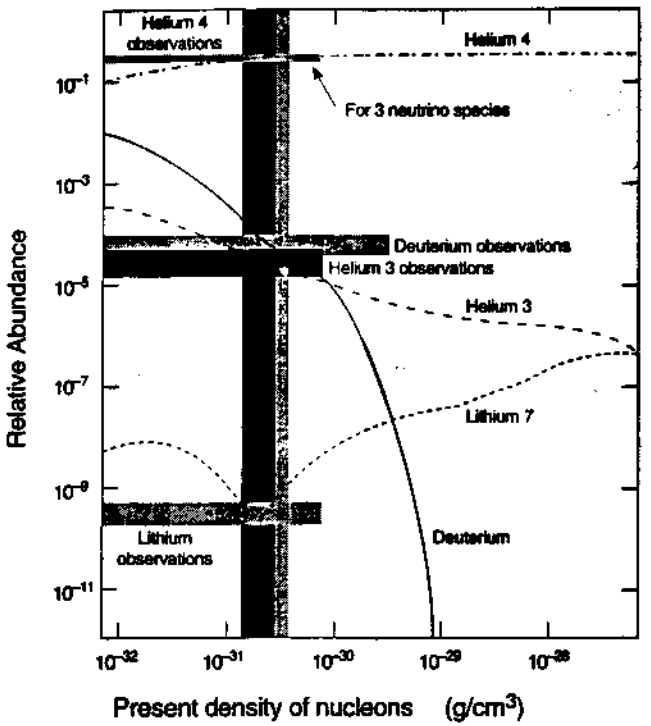
Helium 4 observations
Helium 4
For 3 neutrino species
Deuterium observations
Helium 3 observations
Helium 3
Lithium 7
Deuterium
Lithium observations
Relative Abundance
Present density of nucleons (g/cm3)

Fig. 11

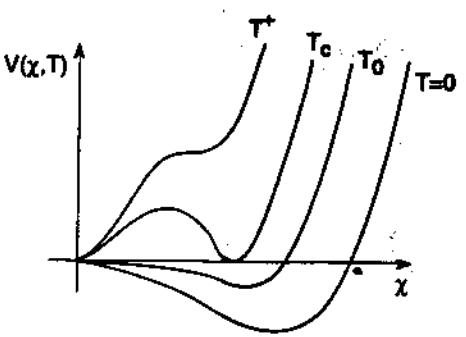
V(χ,T)
T+
Tc
T0
T=0
χ

Fig. 12

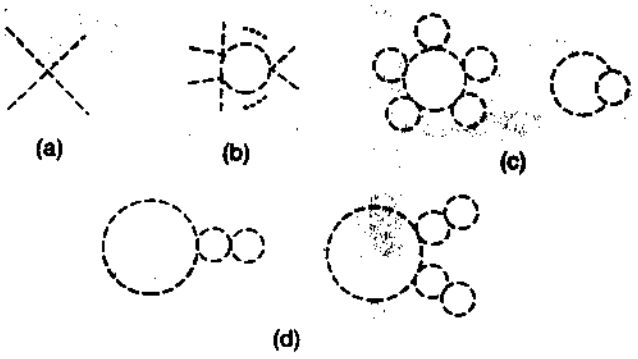

Fig. 13

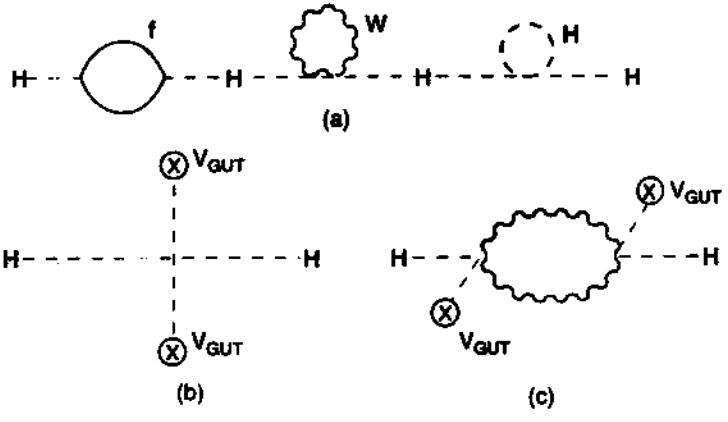

Fig. 14

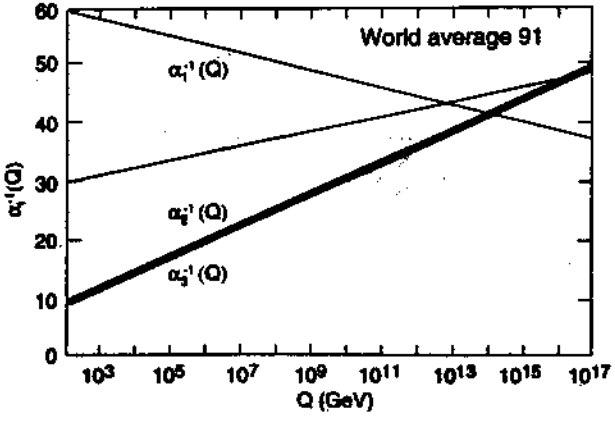
World average 91
$\alpha_1^{-1}(Q)$
$\alpha_2^{-1}(Q)$
$\alpha_3^{-1}(Q)$
$\alpha_i^{-1}(Q)$
Q (GeV)

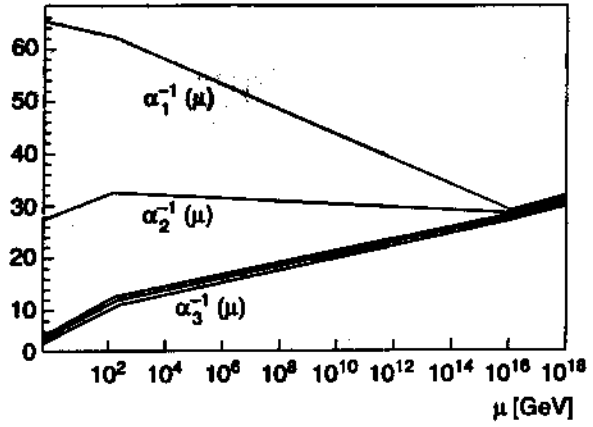
$\alpha_1^{-1}(\mu)$
$\alpha_2^{-1}(\mu)$
$\alpha_3^{-1}(\mu)$
μ [GeV]

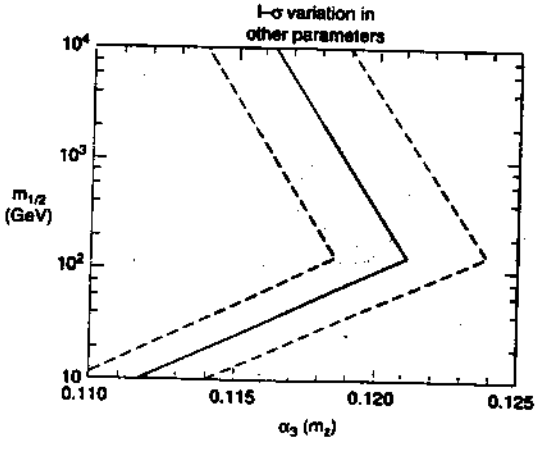
1-σ variation in other parameters
$m_{1/2}$ (GeV)
$\alpha_3(m_z)$

Fig. 15

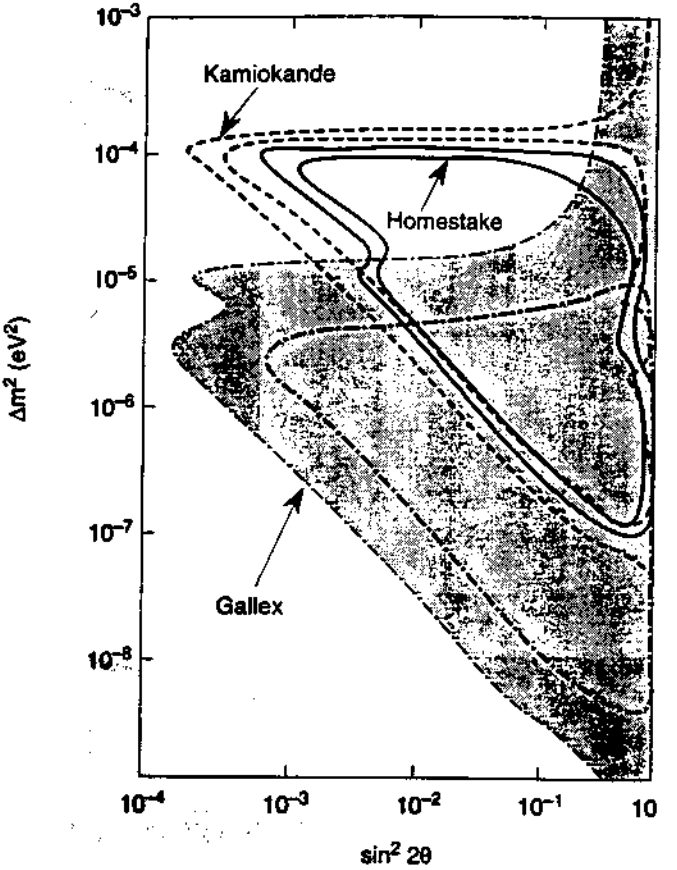
Kamiokande
Homestake
Gallex
10^{-3}
10^{-4}
10^{-5}
10^{-6}
10^{-7}
10^{-8}
Δm^2 (eV^2)
10^{-4}
10^{-3}
10^{-2}
10^{-1}
10
$\sin^2 2\theta$

Fig. 16

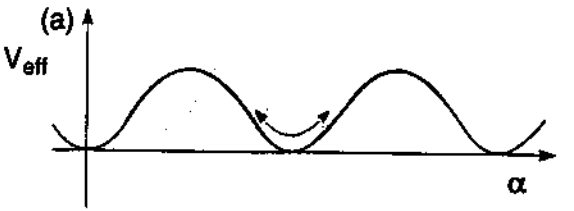
(a)
V_{eff}
α

Fig. 17

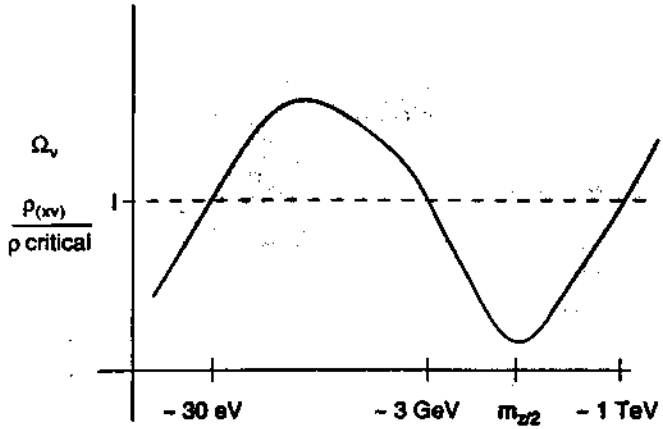
Ω_ν
$\frac{\rho_{(\nu)}}{\rho \text{ critical}}$
1
~ 30 eV
~ 3 GeV
$m_{3/2}$
~ 1 TeV

Fig. 18

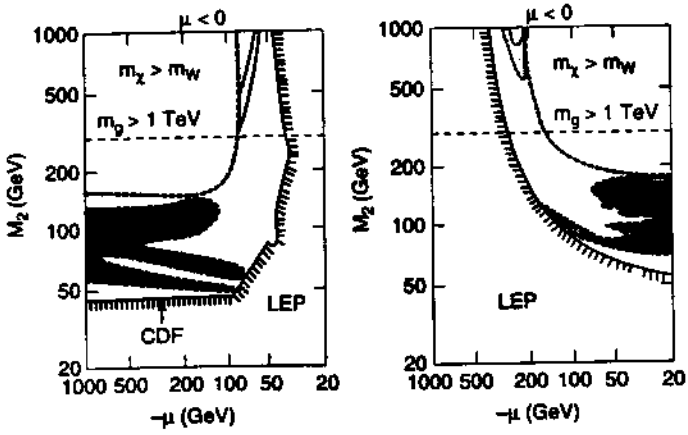
μ < 0
$m_\chi > m_W$
$m_g > 1$ TeV
LEP
CDF
M_2 (GeV)
−μ (GeV)
1000
500
200
100
50
20

Fig. 19

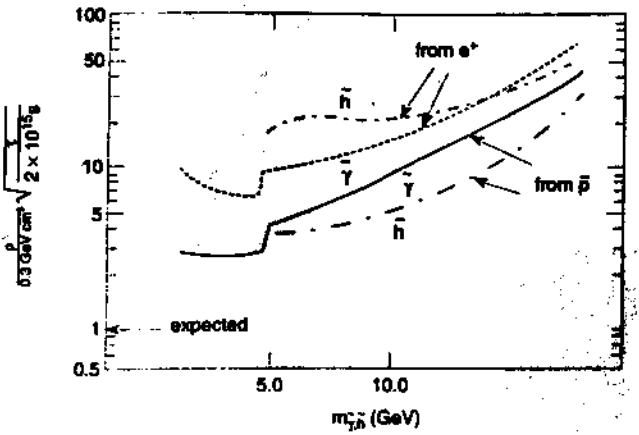
100
50
10
5
1
0.5
5.0
10.0
from e⁺
from p̄
expected
m$_{\tilde{\gamma},\tilde{h}}$ (GeV)

Fig. 20

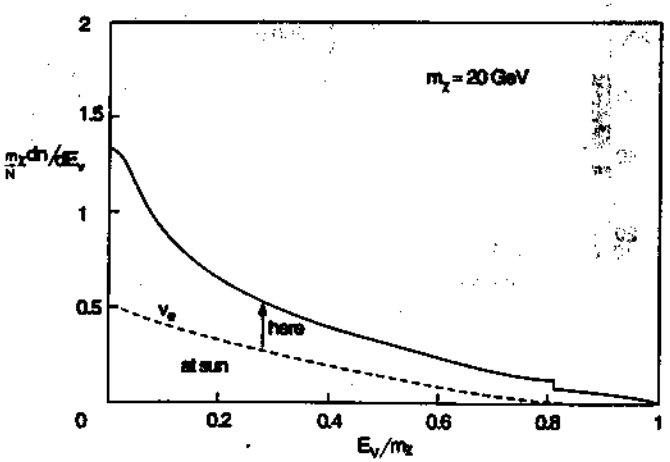
2
1.5
1
0.5
0
0.2
0.4
0.6
0.8
1
m$_{\tilde{\chi}}$ = 20 GeV
ν_e
here
at sun
E$_\nu$/m$_{\tilde{\chi}}$

Fig. 21

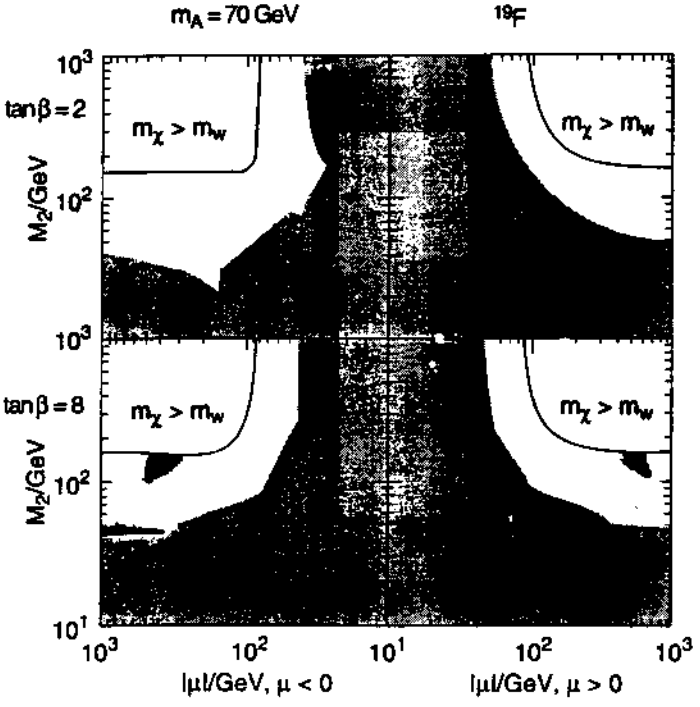

Fig. 22a

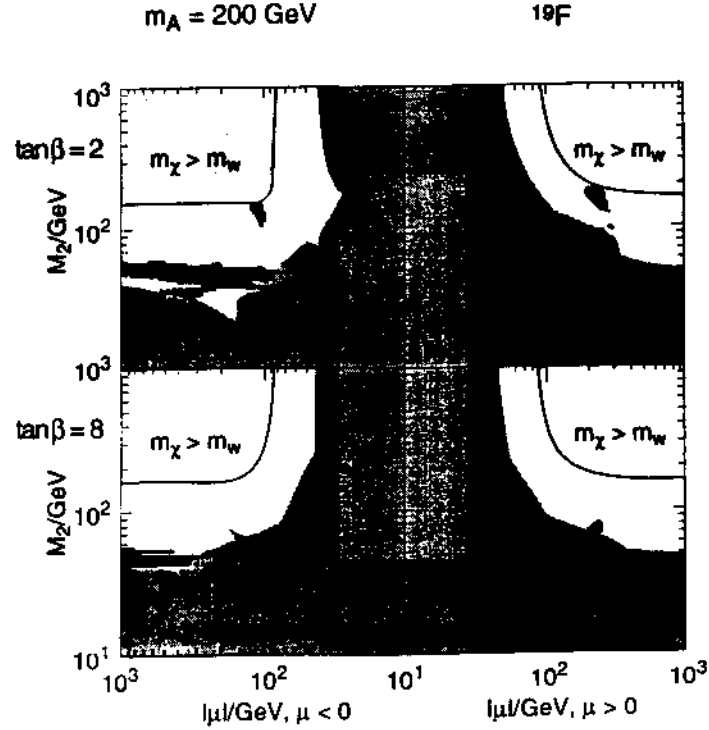

Fig. 22b

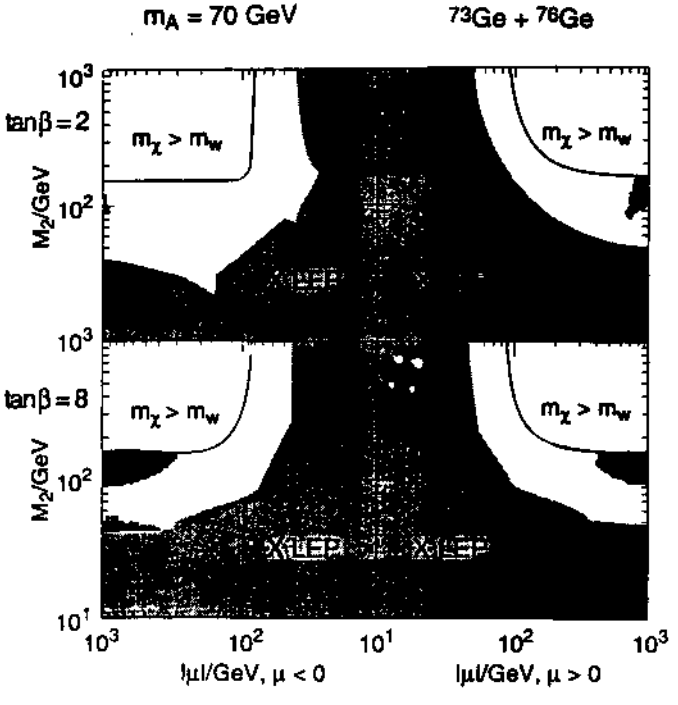

Fig. 22c

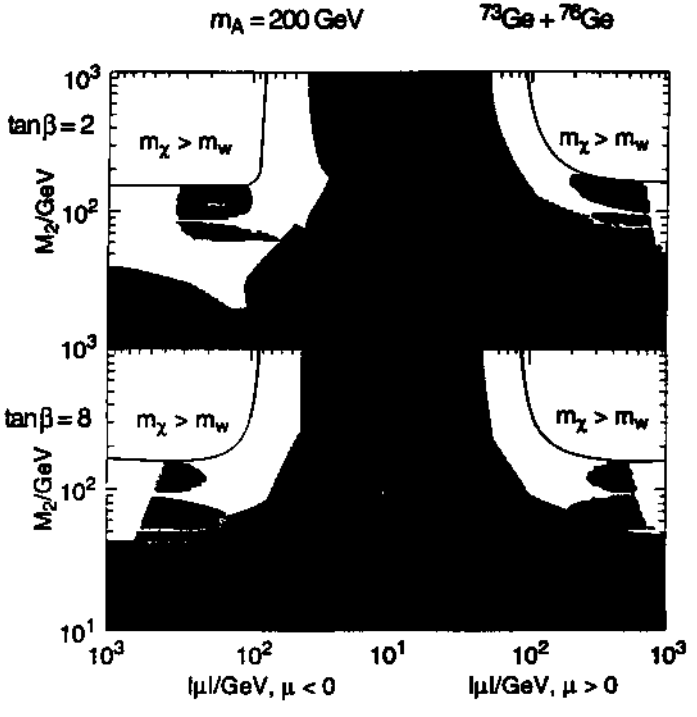

Fig. 22d

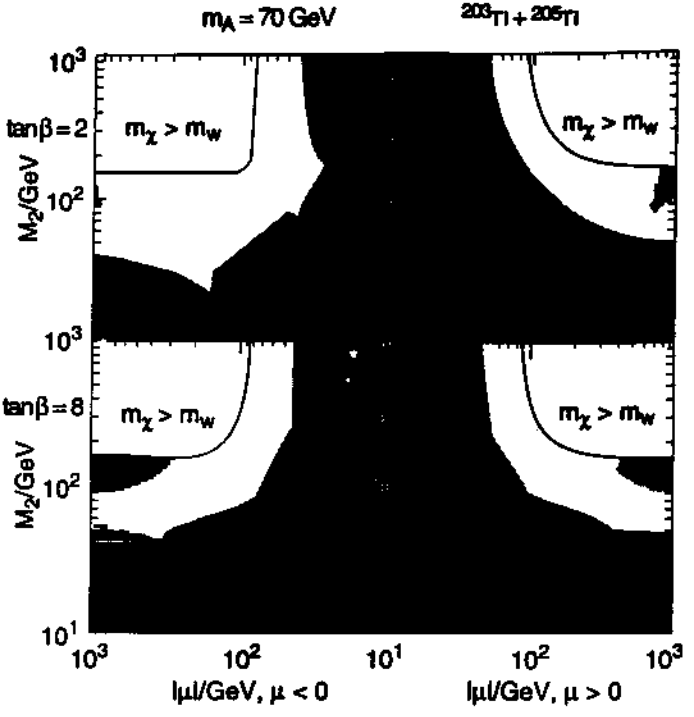

Fig. 22e

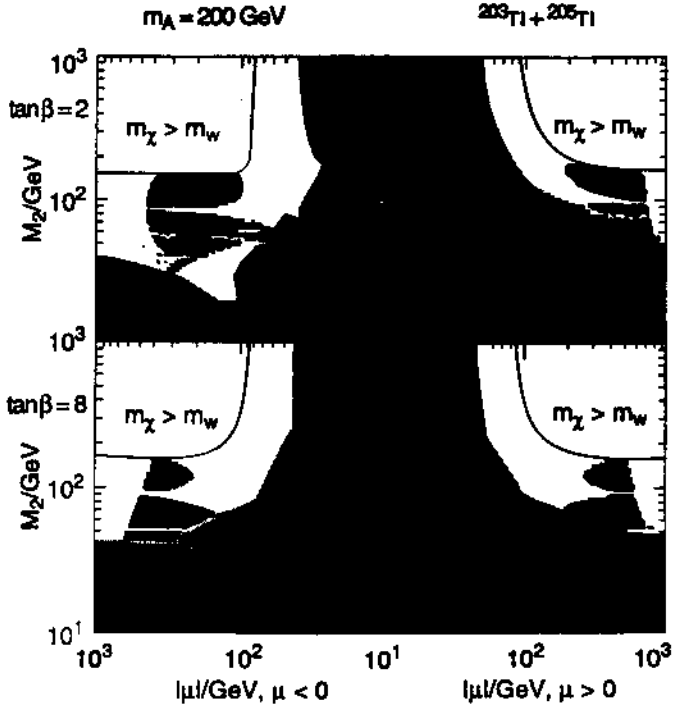

Fig. 22 f

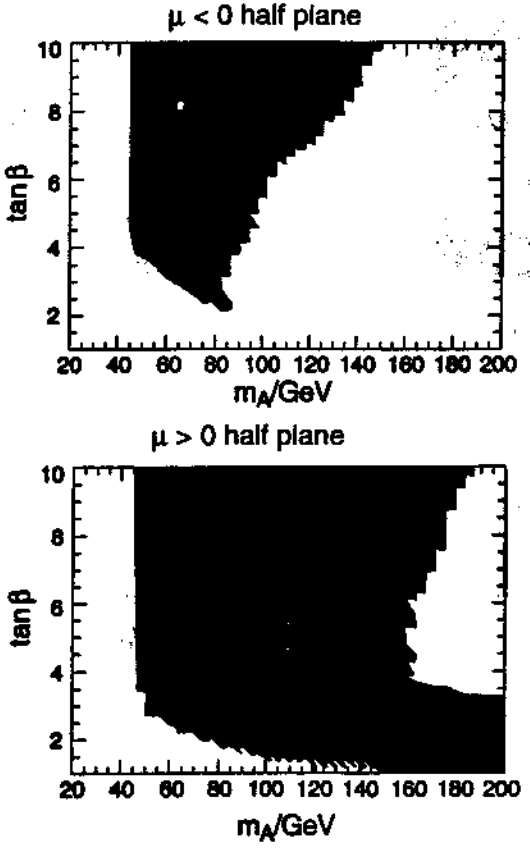
μ < 0 half plane
tanβ
10
8
6
4
2
20 40 60 80 100 120 140 160 180 200
m_A/GeV
μ > 0 half plane
tanβ
10
8
6
4
2
20 40 60 80 100 120 140 160 180 200
m_A/GeV

Fig. 23